Universiteit Leiden

Opleiding Informatica

3D reconstruction techniques to aid biological research

Name:	K.T. Griffioen
Date:	August 14, 2017
1st supervisor:	Prof. Dr. Ir. F.J. Verbeek
2nd supervisor:	Dr. J.H.N. Lindeman

MASTER'S THESIS

Leiden Institute of Advanced Computer Science (LIACS)
Leiden University
Niels Bohrweg 1
2333 CA Leiden
The Netherlands

Master thesis
3D reconstruction techniques to aid biological research

K.T. Griffioen, Bsc.
Supervised by:
Prof. Dr. Ir. F.J.Verbeek & Dr. J.H.N. Lindeman

August 14, 2017

Contents

Abstract

In biology, problems are often addressed in a 2D fashion. Tissues of interest are often cut in extremely thin slices, stained for certain structures and examined using light microscopy. This method has proven to be powerful, but has obvious limitations when it comes to understanding the 3D structure of the structure of interest. This thesis describes the use of 3D reconstruction methods, Computer Science and biological techniques to solve biology-driven research questions. Two different resolution scales have been investigated, with a corresponding biological problem. The first problem has a resolution of 10 μm which we will address as 'meso', whereas the second scale has a μm scale, which we will address as 'micro'. Both of these require a different approach. The main research field of interest was Cardiovascular disease, which is rated as the number one death cause globally. The first disease that fits in the *meso* description was atherosclerosis. One of the processes that is involved with atherosclerosis is the generation of new capillary networks These networks, also known as vasa vasorum, have not yet been reconstructed in high resolution and fits into the 'meso' description. This thesis describes a work-flow to create a 3D reconstruction of such a network which has been visualized as a fly-through animation. One interesting conclusion that could be drawn from this model was that the vast network of vasa vasorum is connected to the lumen of the blood vessel. A second reconstruction has been created of the blood vessel surroundings and is used as an overlay. The methods that were used in this thesis could be re-used for varying reconstruction purposes. These other reconstructions might be used as an addition to the current model as well. The second part of this thesis consists of an investigation into bicuspid aortic valve(BAV) disease. Patients who suffer from a BAV only develop complications in approximately one to two thirds of the patients and most often comes in the form of aortic dilation. The exact mechanism behind the dilation is unclear. In this thesis, we aimed to investigate using 3D imaging techniques and data-mining methods whether BAV patients have a structural defect of the aortic wall. After an extensive search to improve the quality of the microscopic imaging, tissues originating from 19 different patients were stained with Sirius Red collagen stain and imaged using a confocal laser scanning microscope. The highest average prediction scores were gained using Local Binary Pattern(LBP) features in conjunction with a Support Vector Machine(SVM) Classifier. This combination yielded a maximal average score of 0.30 when predicting the class and a maximum average score of 0.70 when predicting only differences of Bicuspid versus Tricuspid patients. To verify the methods we used, the same classification methods have been applied to other cases like Marfan's syndrome and images of the adventitia and media, which yielded a mean score of 0.95 and 0.90, resp., which shows us that these methods have the ability to perform quite well on similar cases. To be able to draw more solid conclusions, more data is needed from more patients. Accuracy of the model will probably increase with an increasing number of patients, and this model could be used to find out if there is a structural defect in the aorta of patients who suffer from BAV, as well as identify characteristics of the defect itself, if found. To perform research as described in this thesis, we need more than image processing alone. The combination between biology and computer science is the key to solving problems in this area.

Chapter 1

Introduction

1.1   Background

Biological research is often conducted in a 2D fashion due to technical limitations in methods. One of the most used methods is to embed tissue of interest in paraffin and cut a very thin slice, which is specifically stained for certain structures and examined using light microscopy. Using these methods, a lot of research regarding pathological processes and tissue compositions has been done. On the other hand, there is one obvious limitation in the case that a researcher wants to understand a process related to the 3D structure of the structure of interest. Using 2D tools, it is very hard to get a correct idea of the exact relationship in 3D.

This thesis aims to investigate into the possibilities and added value of 3D reconstruction methods, which consist of a combination of Biological and Computer Science methods. Two resolution scales will be investigated, which are addressed as the *meso* and the *micro* scale. The meso scale describes structures with a resolution of around 10 μm whereas the micro scale describes structures which are one μm or smaller.

Two different problems from the field of Cardiovascular Diseases (CVD) have been selected that fit into our meso and micro scales, respectively. 3D reconstruction of coronary blood vessels and the capillaries inside them which supply them of oxygen fit the meso description, since capillaries have a diameter of approximately 5-10 μm. For the micro scale, Bicuspid Aortic Valve(BAV) disease has been chosen. A typical problem seen in BAV patients is the dilation of the ascending aorta. This problem shows in approximately two thirds of the patients, whereas the other third never develops these problems. The exact cause of the dilation or weakening of the aortic wall is not known. An investigation into a structural defect will need imaging at the highest level of resolution that light microscopy can give us, being less than a micrometer per pixel.

In this thesis, Computer Science techniques will be used to answer biological questions regarding CVD. To do so, existing tools should be extended, linked and sometimes it is even necessary to produce own algorithms for certain problems. The problems addressed in this work are not solvable by using standardized toolkits right now. There are too much hurdles to be taken which simply are no part of any software package. This is why sufficient knowledge of Computer Science is required on top of biological knowledge about the problem. Some of the images that have been used in this project are too large to

even be fit in memory on a regular workstation (16GB of RAM) since they are 80,000 by 80,000 pixels, let alone be processed in any way. This requires sufficient knowledge about the display capacity and memory requirements of applications. Often used tools for 3D reconstruction are ImageJ plugins for example, but ImageJ has no system which allows for reading only part of an image. Two diseases will be investigated, being atherosclerosis and BAV. Both will be addressed by looking at 3D structures of the tissues. Recently, the more 'macro' 3D structure of a coronary artery with a starting phase of atherosclerosis has been investigated using serial section images which were aligned, segmented and reconstructed into a 3D model. This method revealed the 3D structure of such a vessel including the atherosclerotic lesion [1]. This thesis elaborates on the methods used in this investigation to further increase the understanding of atherosclerosis.

1.2 Microscopy

This section describes several forms of microscopy.

1.2.1 Bright-field microscopy

The simplest form of microscopy is the bright-field microscope. Using a microscope like this, specimen can be enlarged significantly and micro-structures can be reviewed. Light microscopy has been extremely helpful in the past to reveal mechanisms that happen at micro-scales. However, only 2D information is available and when 3D structures are important for understanding certain pathologies, this form of microscopy alone is not suitable. The range of a light microscope is limited as well. Nowadays, there are whole slide scanners available which are capable of scanning the complete specimen using a very high resolution, which means that the complete slide is available digitally which solves the limited range problem. One of these scanners is used in this project as well, which is a model from PHILIPS [2]. This is the first whole slide scanner which can handle a slide in less than a minute and can adapt the focus during scanning. The resolution of such a device is 0.25μm per pixel. Using 3D reconstruction methods it is possible to create a 3D model which can be reviewed in a 3D manner. The limitation of this technique is that it remains a reconstruction, which means there can be errors in the final 3D relationship. Another microscopy technique is fluorescence microscopy. Fluorescence microscopy only shows a limited range of filaments and structures in the specimen because these structures have to be fluorescent or have a fluorescent label attached to them. Light microscopy can use certain stains which stain different structures or tissue types, which means that these specific tissues are distinguishable. A fluorescent microscope is more limited in this aspect. However, using a confocal laser scanning microscope (CLSM), it is possible to capture 3D optical stacks of the specimen, which immediately allows the collection of spatial information. Capturing an image using a CLSM is a very slow process compared to a whole slide scanner, for example, especially when 3D stacks are captured.

1.2.2 Fluorescence microscopy

Fluorescence microscopy is a subfield in the field of light microscopy and it relies on the principle of absorption of light at certain wavelengths which results in the excitation of

certain molecular bonds which then start to emit light to loose their excited state. The emitted light has a lower energy state and thus a longer wavelength. Not all structures are directly visible under a fluorescence microscope. If a structure emits light when excited with a certain wavelength without any labeling, it is said that such a structure or molecule is autofluorescent, meaning that it does not need anything else than to be excited with a certain wavelength to be able to emit fluorescent light. Whenever a structure is not autofluorescent, it might be labeled with a molecule which binds specifically to the structure of interest. This molecule has to be bound to a fluorophore, which is a fluorescent group that can be attached to a molecule. This method makes it possible to review structures that are not autofluorescent.

There are two main types of microscopes used for fluorescence microscopy, a wide-field microscope/epifluorescence microscope and a confocal laser scanning microscope. The principle of the two microscopes is similar, but the confocal uses a laser as a light source instead of a lamp. An example of an epifluorescence microscope setup is shown in figure 1.1. The laser in combination with a pinhole that are both located in a confocal laser scanning microscope (figure 1.2) enables the creation of so-called focal planes, which can be stacked to create a 3D volume render of structures. The great advantage of a confocal microscope is the confined z-space where it can focus. A wide-field microscope can also focus on a certain layer in a thicker sample, but it cannot block out light beams that come from other layers than the focal point. When reviewing thicker slides with an epifluorescence microscope, structures above and below the focal point blur the final image.

1.3 Research Questions

The leading research question of this thesis is about which methods are applicable for which target scale and structure. Two research questions following from the main one are driven by the target scales that are defined for this project. The first research question is about the *meso* scale problem and regards the structure of the vasa vasorum that are generated near an atherosclerotic plaque, what this network of vessels looks like and what methods are applicable to get to a correct reconstruction. The second research question is about the *micro* scale problem which regards BAV disease, whether we can find evidence that BAV is caused by a structural defect in the vessel wall, and if so, what characterizes this defect. Methods that are needed for both problems will probably have some overlap. To answer these questions, several biological tools will have to be combined with computer science tools. A reconstruction of the vasa vasorum is a more difficult problem than the reconstruction of the vessel in [1] since the structure of interest is a lot smaller, contains a lot more detail and thus needs processing at higher resolutions to be reconstructed. New research questions that need to be answered are how to deal with higher resolution layers of microscopic scans, what kind of staining techniques should be used, what kind of segmentation methods should be used and what methods should be used when creating an overlay of two 3D models. In the case of BAV, further research questions that arise are what kind of filament(s) will be subject of investigation, what microscopical techniques will be used and what data-mining approaches should be used to determine differences between tissue classes.
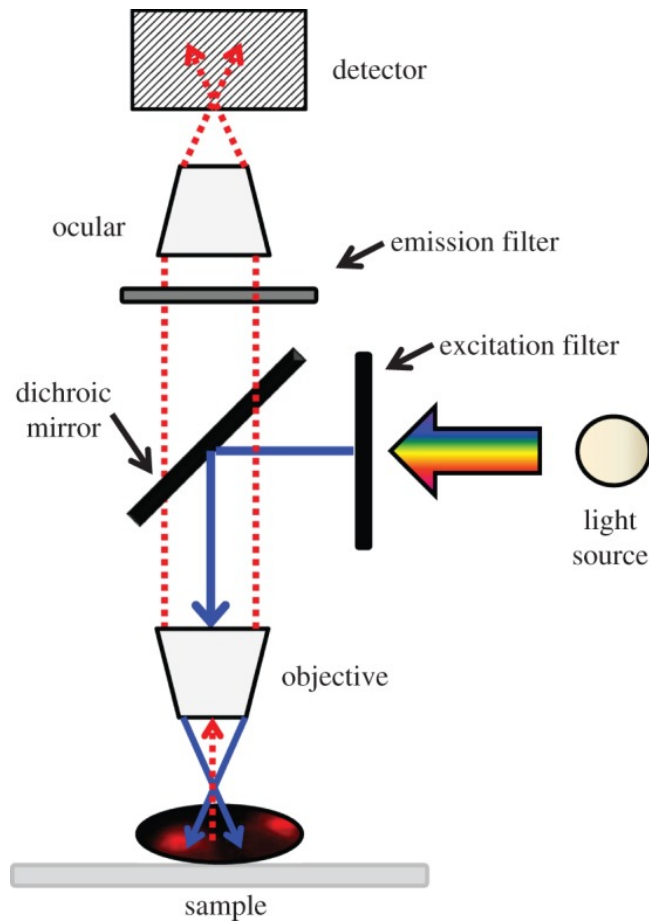
Figure 1.1: Simplified schematic of an epifluorescence microscope (adapted from [3]). Light enters the setup through the lamp at the right, and is directed downwards using a dichroic mirror, where it excites the sample which emits light that passes through the objective, mirror, filter(s) and ocular until it reaches the detector. This is usually a CCD camera chip.
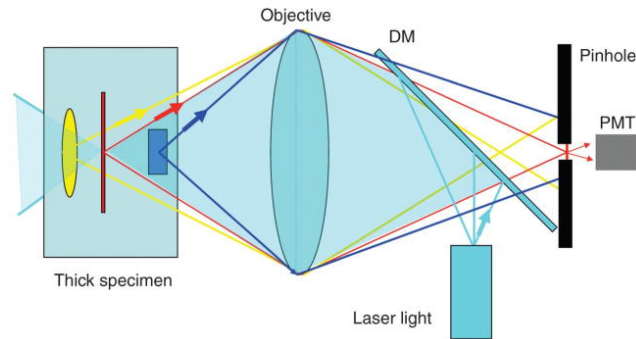
Figure 1.2: Schematic of the confocal microscope (adapted from [4]). The pinhole only allows emitted light from a certain layer inside the specimen to go through the hole. The rest of the signal will fall on the sides of the hole. The size of the pinhole can be adjusted to allow for a larger or smaller focal plane.
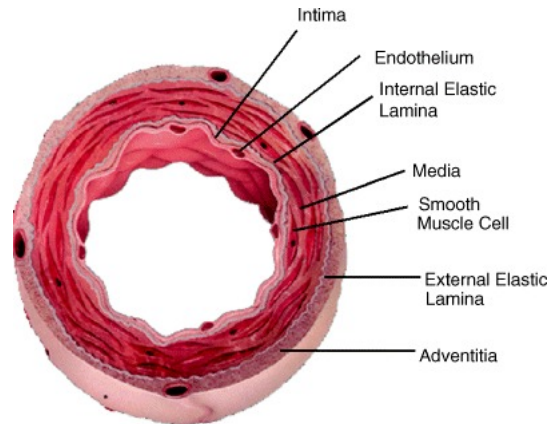

Figure 1.3: Anatomy of the vessel wall. Adapted from [6].

1.4 Clinical background

Coronary Artery Disease (CAD) is the most common heart disease of which 8.14 million people died globally in 2013, making it the leading cause of death around the world [5]. CAD is a member of the Cardiovascular Diseases(CVD), but CAD on itself takes up the number one place in the list of causes of death. The rest of the cardiovascular diseases combined take up place 33. CAD is caused by atherosclerotic processes. The high mortality and prevalence associated with CVD make it an interesting research topic overall. Increase in understanding of the pathological processes involved might in turn increase treatment options.

1.4.1 Vessel wall structure

In this thesis, all research is involved with blood vessels. This section is meant as an introduction to the structure and nomenclature of blood vessels.

A schematic representation of the blood vessel wall is shown in figure 1.3 Blood vessels have a quite common structure, which can be found in arteries as well as veins. The innermost layer of the blood vessel is called the lumen, which is basically one layer of endothelial cells. The lumen is part of the intima, which comprises not only the innermost layer of endothelial cells, but a thin layer of connective tissue. This intimal layer is surrounded by the medial layer which mainly consists of smooth muscle cells, elastin and collagen fibers. The medial layer is the thickest layer in arteries. Separated by the external elastic lamina, the third and outer layer of a blood vessel is the adventitial layer. This layer consists of connective tissue only. In veins, this layer is the thickest layer of the three. Capillaries only consist of a layer of endothelial cells, and sometimes a small layer of connective tissue surrounding it.

1.4.2   Atherosclerosis

Atherosclerosis is a slowly progressive disease which is caused by the accumulation of lipids in the inside of blood vessels. This is a complex process which involves a lot of different substances and inflammation processes [7,8]. In the very first stage, Low Density Lipoprotein (LDL) particles enter the semi-permeable vessel wall and settle in the intimal regions. This LDL deposition will initiate inflammatory responses, which in turn attract macrophages which will try to clean up the LDL molecules. However, the surplus of LDL that is present will cause them to continue to 'eat' LDL until they die. Macrophages which have consumed a surplus of LDL cholesterol have come to be known as 'foam cells', since they have a foam-like appearance. The ongoing inflammation processes and accumulation of LDL molecules create a more complex lesion which also triggers pathways of smooth muscle cells that will be produced and combined with collagen, to produce a fibrous layer on top of the existing lesion. Since foam cells continue to die in this stage, a necrotic area will be generated as well. This fibrous tissue is also known as an atherosclerotic cap. The necrotic area is known as the necrotic core. Over time, this necrotic core will grow larger and eventually contain a mix between lipid crystals, cell debris and necrotic cells. In time, this means that the blood vessels intimal regions which become significantly bigger, containing more and more fatty substances and inflamed tissue. The vessel itself suffers from decreased flexibility because of the fibrous cap.

Whenever this process is allowed to continue, the opening of the blood vessel will become smaller and smaller, up until a point where the blood flow can become a problem. Hypertension is observed within patients who suffer from severe atherosclerotic lesions. Angina is a common symptom related to the narrowing of blood vessels. Angina can cause problems like ischemia (cells dying due to lack of oxygen) over time since the blood vessel wall thickens and gets more rigid. Hypertension and angina, however, are not the biggest problems. A more serious problem is a partial rupture of the cap of an atherosclerotic plaque [9], which allows thrombogenic substrates to collide with the cholesterol/fat crystals and necrotic areas in the necrotic core which immediately attracts platelets which aggregate, cause a chain reaction. The result is a blood clot inside the vessel. The blood clot will become bigger and bigger up until the point where it clogs up the complete artery (or vein). When a clogging like this happens in a coronary vessel, the person would suffer from a heart attack, since blood cannot pass through the vessel anymore, leaving (part of) the heart without any oxygen supply. A heart attack can vary in severeness, based

on the location of the attack and thus the location and size of the heart that is cut off from oxygen supply. The obstruction can also be incomplete, in which case the immediate results are less severe than when the obstruction is complete. However, if such a thrombus detaches and travels through the vascular system as an embolus until it gets stuck in a smaller artery, it will create an obstruction there, possibly resulting in stroke or myocardial infarction due to ischemia. Such infarction can lead to cardiac arrest. If cardiac arrest occurs and no Cardiopulmonary resuscitation (CPR) is applied, this person will die. Atherosclerosis in the regions of the brain can lead to stroke due to similar processes.

1.4.3   Angiogenesis

Angiogenesis is the generation of tiny capillaries to supply a region of oxygen [10]. Angiogenesis can occur in the inside of the vessel wall after the inflammation and fatty streak of these regions, to provide the aortic wall with oxygen and mediate in inflammatory processes. This process is also known as neovascularization. Normally, the vessel wall is provided with oxygen through the adventitia. This is possible because the wall is quite thin and oxygen can freely diffuse through the aortic wall. However, with the thickening of the wall, the distance becomes too great at some point such that a renewed oxygen supply is needed. This will initiate pathways which lead to the generation of new blood vessels (neovascularization). Capillaries inside the vessel wall are known as vasa vasorum. These capillaries can occur in normal vessels, but in the case of atherosclerosis, vast, dense networks of these capillaries are generated. Plaque growth is also related to angiogenesis [11], as the capillaries act as a portal for inflammatory cells.

1.4.4   Bicuspid Aortic Valve disease

In addition to the previously mentioned cardiovascular diseases, Bicuspid Aortic Valve disease (BAV) is the most common congenital heart disorder [12]. A normal aortic valve consists of three cusps (see figure 1.4), which will open and close to allow blood to flow through, or prevent it from flowing through. This is one of the bases for the correct contractions of the heart, and the correct blood flow of the heart. Patients with this disease have an aortic valve that consists of 2 cusps instead of the 3 that the aortic valve normally consists of. This abnormality is present at birth. During the developmental phase, two cusps out of three are fused together, which explains the raphe that is most often visible in the middle of the bigger cusp. The fact that BAV patients have only two cusps in itself does not appear to be problematic since the valve can function reasonably normal in most cases, but there are reports about this type of valve that suggest that it leaks sooner than a tricuspid one because of the changed morphology.

In one third to two thirds of BAV patients, problems will arise in later stages of life [12,13]. There are numerous reports of patients with a BAV which develop complications in adulthood, where the most occurring complication is the dilation of the ascending aorta which often evolves into an aneurysm of the ascending aorta (AAA). AAA often results in a rupture if untreated. A rupture of the aorta is a very severe diagnosis which is only successfully treated for the first time in 1951, and has nowadays improved to have a mortality of only 4% using the EVAR technique [14].

The BAV problem raises a few interesting questions, such as why some BAV patients

develop this dilation of the ascending aorta, and why some of them do not. Two main theories have been proposed, where the first is that the reason for the frequently occurring dilation of the aorta is the altered morphology of the valve, which is thought to have a different blood-flow as an effect. This blood-flow would then interact with the aortic wall in the form of shear stress, which would induce a vascular remodeling of the aortic wall. The second theory states that BAV disease is a more complex disease than it seems beforehand, and not only limited to changes in the aortic valve itself. BAV is a genetic disorder, which could have more extensive complications and might cause an abnormal structure of the aortic wall as well.

The investigation into BAV disease has been subject to controversy for years. Even up until now, both theories receive support. In 2002, Fedak et al. [15] reported that the vascular complications were not related to a dysfunctional valve. More than 50% of young patients have normal functioning valves but show dilation of the ascending aorta. Whether this statement is true has also been subject to considerable controversy [15]. Fedak et al. also reported that the comparison between the aortic tissue samples of BAV patients and tricuspid showed degradation that was similar to that of fibrillin-1-deficient aorta, and the collagen and elastin levels inside this aorta were at normal levels. In 2003, they published a study which showed that the amount of fibrillin-1 in the aortic wall is in fact lower [16] compared to patients with normal tricuspid valves. The mechanism involved has been proposed as well, which is shown in figure 1.5. A deficiency of fibrillin-1 results in increased matrix metalloproteinase (MMP) matrix fragmentation which in turn would reduce the structural integrity of the vessel wall. This study [16] is cited in reviews afterwards, for example by Tadros et al. in 2009 [17], Siu et al. in 2010 [12], Losenno et al. in 2012 [13] and Verma et al. in 2014 [18]. The review of [13] remarks that it is not clear whether the fibrillin-1 is the cause of the degradation and dilation of the aortic wall, or a result of these processes. This review also states that the flow reportedly is not normal despite the BAV is functioning normally, which might indicate that the flow can still be the cause of the dilation of the aorta in these cases. Another remaining question is why some BAV patients develop this dilated aorta, and some do not.

Even in 2011 [19] and 2012 [20], the relationship between aortic valve dysfunction and AAA has been investigated again within BAV patient groups. This shows that there is still little convincing evidence available, even concerning the relationship between valve dysfunction and AAA.

As mentioned before, neither of the theories have been proved or disproved until now. The shear stress theory might sound the most straightforward and logical of the two since the most visible proliferation of a BAV is the altered morphology of the valve, but evidence about the alteration of the flow and the negative effects thereof is still lacking. This is why some reviews conclude that the aortic dilation is not caused by an altered morphology, since patients with a normally functioning bicuspid valve show severe dilation as well.

When looking at aneurysms in general, there seem to be two main types of aneurysm growth and tissue degeneration. The first type is an inflammation-mediated degeneration, the second is best described as an hereditary defect, which is a type of degeneration that is not related to inflammation processes [21]. BAV disease is frequently compared to Marfan's disease [15–17] because of it's histological similarity. The aneurysm growth seems comparable with BAV as well, and is not inflammation-mediated. Marfan's disease
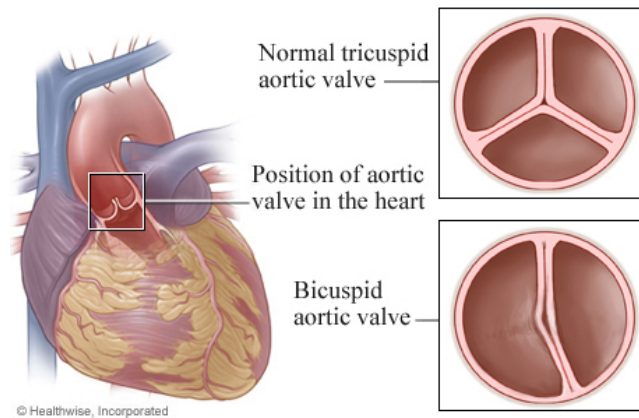
Figure 1.4: Bicuspid aortic valve compared to tricuspid aortic valve. Adapted from `http://www.webmd.com/heart/bicuspid-aortic-valve`.

is reported to have a severely disrupted collagen matrix [22]. Since the histology is similar, similar pathological processes might apply in this case as well.

Most of the research that has been done focuses on the visual observation of valve and aortic material, as well as microscopic evaluation of these tissues, including specific stains for certain structures within the aortic wall and several determinations of quantity of structural filaments like the fibrillin-1 that is discussed above. However, these methods do not reveal any structural relations in 3D, while spatial relations and reconstructions can be very informative, as was the case in [22] for example.

In this thesis, we will be looking at a setup for a 3D-oriented experiment, as well as some experimental data and results which might serve as a step towards a more solid conclusion regarding the BAV problem. The included investigation aims to use 3D imaging techniques to find out whether the elastin and collagen matrix is disrupted, if we can use data-mining methods to determine this, and whether a structural defect of elastin and collagen could be the cause of AAA in BAV patients.
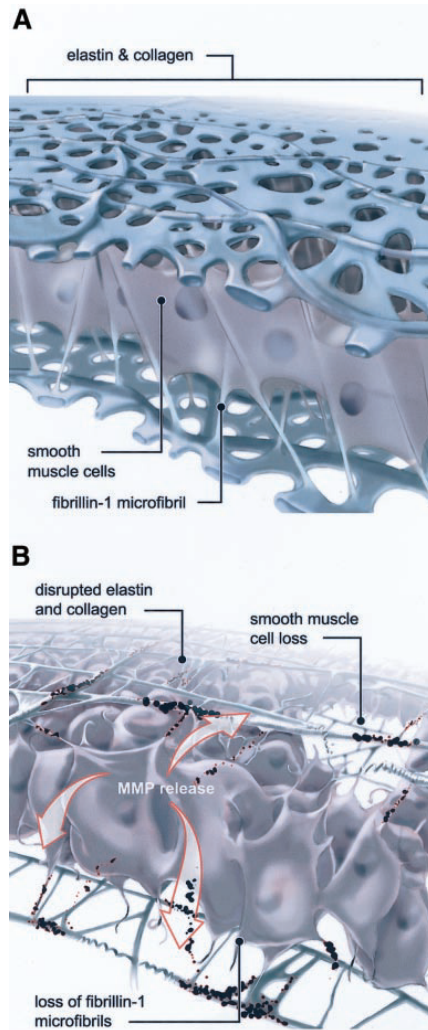
Figure 1.5: Proposed mechanism for dilation and degradation of aorta in patients with BAV. Adapted from [15]. In normal tricuspid valve patients (A), the fibrillin-1 micro-fibrils tether the smooth muscle cells to elastin and collagen filaments. In patients with BAV(B), these fibers are deficient and are not able to correctly function. This causes MMP release, cell death, matrix disruption and loss of structural support.

Chapter 2

Materials and Methods

During this thesis, we have tried to work according to the work-flow shown in figure 2.1. The main focus lies on the combination of biological and computer science techniques. For example, computer science methods can be used to extract information like the location of atherosclerotic lesions from microscopical images using complicated machine learning techniques which cost a lot of time to train. However, using biological methods, it is possible to stain specifically for these regions, creating a clear contrast for these areas, which can be easily extracted based on color using computer science methods and algorithms.
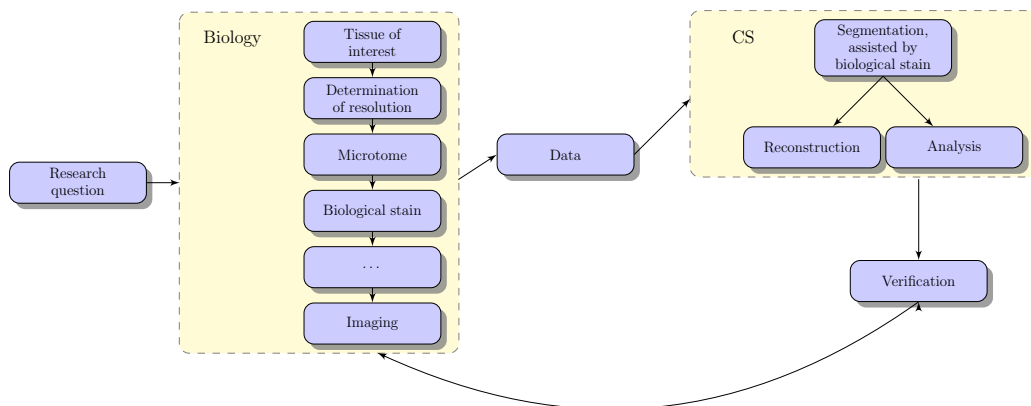

Figure 2.1: Work-flow that is the basis for this thesis.

2.1 Software

A range of software packages have been during the course of this thesis, which are listed in table 2.1. Existing tools were extended upon and linked using bash, python and Matlab and the scripting environment of ImageJ. Since this thesis was an exploratory search into 3D reconstruction, the goal of this thesis was never to create a comprehensive, high performance software package with low memory usage. Such an approach would take too much time and offers too little flexibility. The focus of this thesis was directed towards

Table 2.1: Software packages used in this thesis.

Software name	Use
Matlab / Octave	Matlab has been used for a major part of all the work that has been done during this thesis. The major parts of image processing have been done using this software as well as bridging between different software packages and operations.
ImageJ (FIJI)	registration, triangulation, segmentation [23]
TDR	Reconstruction, triangulation, visualization [24]
VIPS/imageMagick	Image processing, interaction with OpenSlide [25]
OpenSlide	Handling the Philips file format [26]
OpenSeaDragon	Visualizing 2D slides
Blender	Visualization [27]
Ilastik	Segmentation toolkit [28]
Python	Analysis, machine learning and data mining
Sci-kit learn	Machine learning library [29]
Bash	For image processing purposes, bash scripts were often used to automate certain conversion procedures.
Zeiss Zen software suite	Inspection of images

the creation of a work-flow that can be used to accomplish 3D reconstructions of tissue using the strategy of linking existing software packages. Some software has been developed during the course of this project, but it was never a goal in itself. In the future, such a software package can be developed based on the work-flow found within this project.

2.2 3D vessel reconstruction

For the reconstruction of a capillary network inside a vessel with an atherosclerotic lesion, we decided to use consecutive sections from paraffin-embedded tissue. The work-flow was the same as described in [1]. This project elaborates on the previously mentioned project. We have used 100 consecutive sections for the vessels in this case. This reconstruction was meant to be used as overlay for the reconstruction created in [1], but due to errors in the numbering of slices, this project contains a complete newly performed experiment. The same procedures have been used as before. All sections were stained using the Ulex stain which stains the endothelium a solid brown color. The nuclei have been stained as well using hematoxylin which is needed by the scanner to focus. An example of a scan of an Ulex/hematoxylin stained slide is shown in figure2.2. The Ulex stain is very specific. This will significantly reduce the complexity of the segmentation and allows us to mostly automatically segment the capillaries. For registration and segmentation, ImageJ was used. The final reconstruction was created using ImageJ as well. Afterwards, to complete the overlay, every 5' slide was re-stained with Movat's Pentachrome to indicate the outline of the atherosclerotic plaque and other filaments, in accordance with the previously mentioned project. Note that this stain was more difficult to perform than the previous
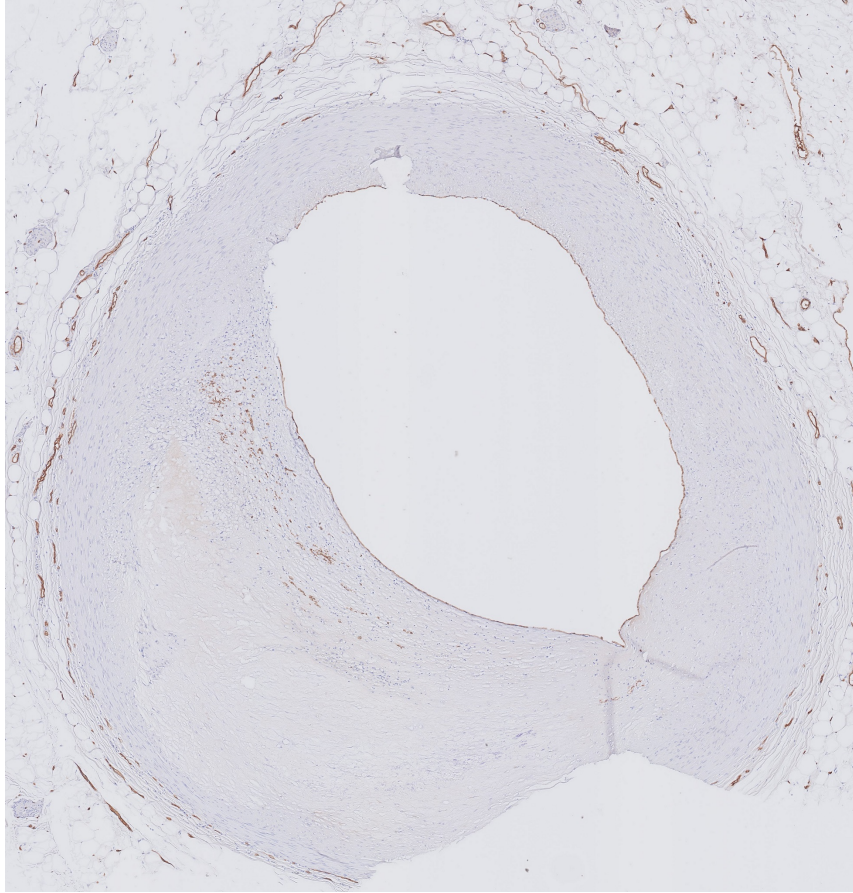
Figure 2.2: Ulex and hematoxylin stained slide scan. Endothelium in **Brown**, nuclei in **blue**. Original tissue originates from a coronary artery, embedded in paraffin. Thickness is 4μm. This particular image contains a significant amount of inflammation cells and vasa vasorum, and an atherosclerotic lesion.

project since the slide was mounted in between. The mounting medium has been dissolved by incubating the slides in Xylene overnight. The cover glass was removed and the Movat stain was applied. The Ulex stain is quite specific and stains only endothelium, so there is no need to remove the Ulex stain from the slide first.

2.3 Bicuspid Aortic Valve disease

Designing an experimental setup for a disease case like BAV is not as straightforward as designing an experimental setup for a certain reconstruction (depending on what structure is the target of reconstruction), as there is no clear understanding of the cause this disease. It is not clear where exactly to look for abnormalities. To determine a region of interest, we have compared BAV with similar diseases which also included the weakening and widening of the aortic wall as pathological process. As mentioned before, a good example would be

Marfan's disease [22], where Lindeman et al. discovered distinct defects in the collagen network. This is one of the most important structural elements of the aortic wall, together with elastin and actin (smooth muscle cells). We decided to look at all three filaments, if possible. Collagen has been visualized using the same methods as [22], where slides were stained using Sirius red. Elastin has been visualized using it's strong autofluorescent signal at 488 nm [30]. This leaves actin, which has be visualized using phalloidin [31, 32] and using an antibody. Collagen can be visualized simultaneously with elastin, but phalloidin does not seem really compatible with Sirius red. The final stain used was a combination of Sirius red to indicate collagen and autofluorescence for elastin. A more detailed description of the search for the correct combination of fluorescent stains can be found in section 3.

To be able to recognize differences between tissue sections, data-mining methods have been used. Based on the fluorescent images that have been produced which were processed into two feature sets. The first set was generated using several handcrafted features, the second set contained Local Binary Pattern(LBP) features which are used more often for image classification purposes. Using these features, models have been trained and tested to determine whether there were significant differences between the different patient groups.

2.4   Equipment

Paraffin sections were cut using the Leica RM2235 microtome in combination with the Leica RM CoolClamp to prevent fast heating up of the paraffin block. The paraffin block was cooled down to -20 degrees Celsius, to improve the quality and reduce the chance on torn tissue sections. Cryosections were cut using the Leica CM1950 cryostat. Several microscopes were used in the scope of this thesis. The whole slide scanner of PHILIPS was used to create whole slide microscopic scans of tissue. The fluorescent confocal laser scanning microscope that was used was a Zeiss LSM5 Exciter upright model. The two-photon fluorescence microscope that has been used is the Zeiss LSM 7 MP.

## 2.5   Histological and fluorescent stains

This section lists all histological and fluorescent stains has been used in this project. Movat's Pentachrome [33, 34] is widely known within the fields of pathology and surgery. It is a very elaborate stain which allows researchers to look at a range of different filaments simultaneously. An example of a Movat stained slide is shown in figure 2.3. This figure shows us the extent of the stain, since the most important filaments for a blood vessel like muscle, collagen, elastic fibers are stained. For atherosclerosis in particular, the blueish stain that will stain areas that contain mucin are very interesting since fatty areas will be stained by that color, which gives a great contrast since the color is a very clear and bright cyan. Ulex [35] is a very useful stain which stains the endothelium of blood vessels. This stains bonding mechanism is chemical, and thus easy to apply and very specific. Sirius red [36] has been used as a wide-field light microscopic stain, as well as a fluorescent stain. Sirius red stains collagen fibers, as well as muscle fibers. The interpretation of the different colors is shown in table 2.2. Phalloidin [31, 32] is a fluorescent actin stain. The exact fluorochrome that is used is Phalloidin-647 and can be excited using a 633nm laser. A mouse monoclonal anti-actin antibody has been used as well, with a secondary antibody
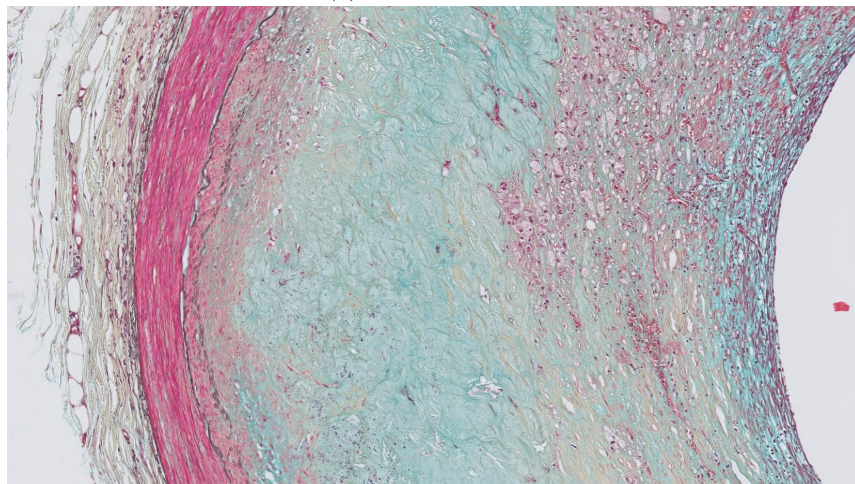
Table 2.2: Sirius red stain interpretation

Histological interpretation	Color
The nuclei	yellow
The cytoplasm	yellow
Collagen fibers	red
Muscular fibers	yellow
Red blood cells	yellow

bound to a 647nm-fluorochrome. This means that this antibody could be excited using the same laser as Phalloidin.
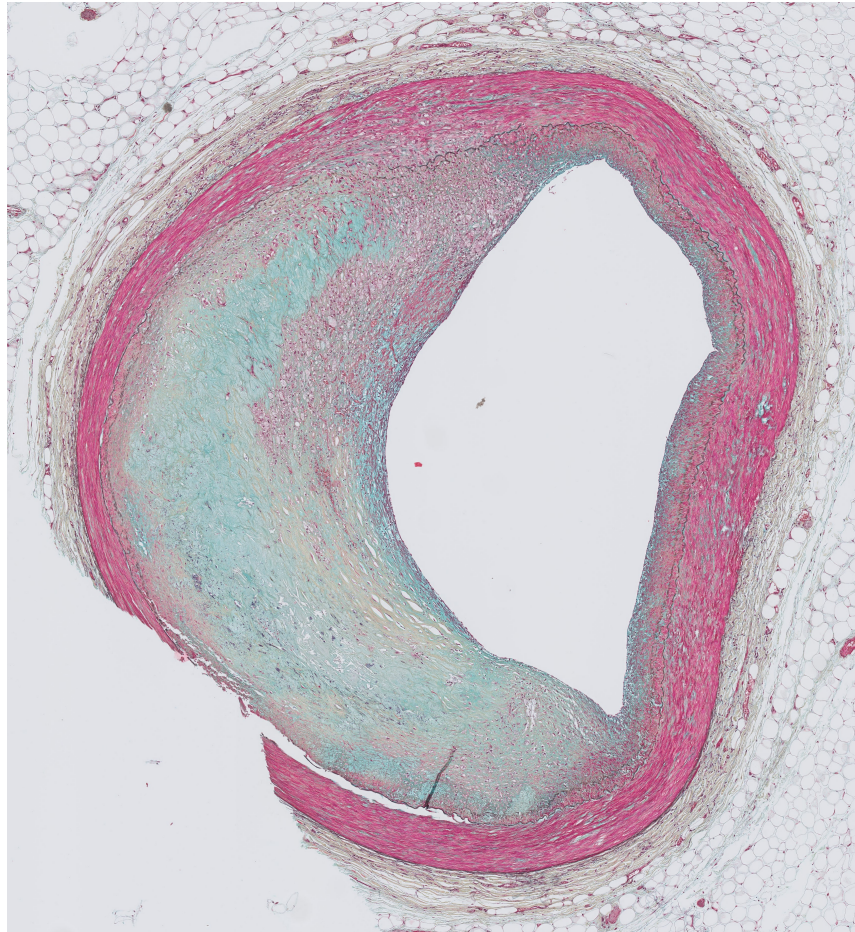
(a) Complete vessel

(b) Cutout

Figure 2.3: Movat stained slide. Original tissue originates from a coronary artery, embedded in paraffin. This particular image contains a moderately severe atherosclerotic lesion. Thickness of the slice is 4μm. Elastic Fibers in **Black to Blue/Black**, Nuclei in **Blue/Black**, Collagen in **Yellow**, Reticular Fibers in **Yellow**, Mucin in **Bright Blue**, Fibrin in **Bright Red**, Muscle in **Red**

Chapter 3

Results & Discussion

Normally, results are listed and discussed later. This section contains results and a discussion because of the size and structure of this section. To avoid references to results reported pages back and explaining afterwards why certain decisions have been made along the way, we have decided to elaborate on the results a bit more and summarize these in the conclusion section. In the course of the project, the work-flow shown in figure 2.1 was leading. We have tried to solve computer science problems using biology and vice versa.

Two problems have been chosen at both the *meso* and *micro* scale. Both these problems require a different microscopy approach. The advantages and disadvantages of bright-field microscopy have been listed in table 3.1. Using this table as a reference, the correct microscopy form can be selected for each problem. A checklist has been included in Appendix B which describes important aspects of a 3D reconstruction process.

3.1 3D model reconstruction

This section describes the *meso*-investigation, which contains a reconstruction of a network of vasa vasorum which are located in the wall of a coronary artery which contains atherosclerosis and contains a macro-overlay of the coronary artery and atherosclerotic plaque. This project is meant as an elaboration of an earlier project which comprised the 3D reconstruction of a coronary blood vessel [1]. Reconstructions like this can give interesting insights in phenomena regarding 3D structure of tissue or localization of certain structures. For example, the previous reconstruction of [1] revealed that holes occur in the muscle wall, all at one side of the vessel. When viewing one slide at a time, such a fact is hard to recognize, since the view is a lot more restricted. The images are not aligned, and the section image has to be interpreted by the viewer.

3.1.1 Capillary reconstruction

One hundred slices have been cut using a microtome from a paraffin block that contained three coronary arteries. All sections were cut at a thickness of 4 μ, since this yields the optimal slice quality with the least amount of damage. The paraffin block was frozen at a temperature of -20 degrees Celsius. Since 100 consecutive slices are quite a lot, this process has to be executed with quite some speed, since the microtome room was

Table 3.1: This table describes advantages and disadvantages of microscopy methods used during this thesis.

Microscopy method	Advantages	Disadvantages
Bright-field microscopy	Stains can be extremely elaborate	Hard to separate specific filaments
	Imaging part is simple	Somewhat wide focus range
	Lots of stains are available	2D
Widefield microscopy		Small range
Whole slide scanner	Wide range, whole slide is scanned in high resolution.	Significant amounts of data
Fluorescence microscopy	Specific signal	Everything that is visible in the end result has to be stained
	Very detailed images	Autofluorescence can interfere with spectrum
		Generally harder to combine stains
Widefield scanner	Range	No optical stacks
	Speed	Significant amounts of data
Confocal	Ability to create optical stacks	Very slow
		Requires significant amounts of knowledge
		Limited range

at room temperature. This meant that after a few minutes, the paraffin block would reach a temperature where the performance of the microtome decreased such that damage occurred to the resulting slice. When this temperature was reached, the paraffin block was returned into the freezer to cool down, until it was cold enough to resume. There are some disadvantages to this method, since a few slices have to be cut from the block when it is taken out of the freezer to ensure a complete slice. This ultimately results in a missing part in the final model. Even small missing pieces in a slice or folds of torn pieces of tissue will result in decreased continuity in the final model. To reduce the number of gaps and occurrences of damage, two people have worked together to increase processing speed of slices. Even so, two of these 'gaps' occurred in this project. This problem might be solvable by moving the microtome into a -20 degrees Celsius environment.

All intermediates of the complete process which is described below and comprises registration and segmentation are shown in figure 3.12, which corresponds to the flowchart of figure 3.9.

All slides have been stained using the Ulex endothelium stain and the haematoxylin nuclei stain as a reference point for the scanner. These slides were scanned in using a PHILIPS high resolution whole slide scanner. The output resolution was approx. 60,000 to 100,000 pixels square for each section. Even though the final region of interest is quite small compared to the complete scan (figure 3.12a compared to figure 3.12f), being approximately 1000 by 1500 μm, data reduction is a necessity due to memory and processing limitations.

Data reduction

The work-flow is based on the methods used in [1] which were adapted to fit the purpose of this project. All images were resized by a factor of 4 using VIPS, which can read the pyramidal tiled TIFF and extract a certain layer from it, which would be layer 2 in this case. This extraction was needed, since these images cannot be loaded directly into memory on the regular workstation that we used, which has 16GB of RAM. The pyramidal TIFF has a resolution factor of 2 for every layer, so the second layer is 2 times smaller than the first. If we extract the third layer, the final result will be $2^2 = 4$, which is an image of approximately 20,000 pixels square. Since every image contained three coronary arteries, every image had to be cropped at first. Using VIPS, these two operations can be performed simultaneously which allows for an enormous reduction in memory usage, disk usage and runtime, because less data is needed from the original image. The command that is used for VIPS to extract a specific region of this layer is shown below.

```
vips crop big_image.tiff[layer=3] 1350 1600 1000 1000
```

This command extracts a 1000 by 1000 sized region from the third layer, starting from the coordinates (1350,1600). This command has been implemented in a Matlab script which has been used for the first cropping step. The script is shown in listing 2 in appendix A. This script shows a low resolution layer of every TIFF file in the indicated folder and allows the user to crop the correct vessel from every image. The coordinates are transformed into the correct coordinates for the layer that is specified and the TIFF files are cropped to the selected area in that layer. During the cropping process, the coordinates are stored in an object on disk as well. This allows for exact reproduction of the selected areas afterwards,
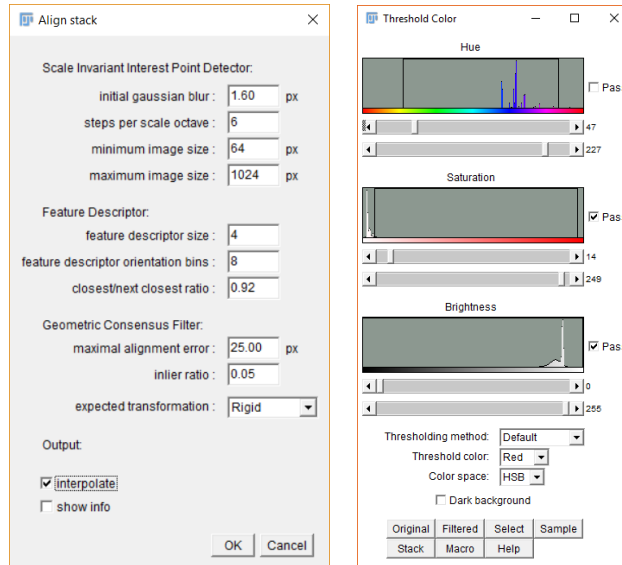
(a) SIFT settings for the align stack plug-in

(b) Typical threshold values for the color threshold plug-in

Figure 3.1: ImageJ plug-in settings used for registration and segmentation of the capillaries.

in any layer that is requested. Also, whenever the cropping fails due to some reason, the cropping process can be resumed from that point.

Registration

Registration was performed using several ImageJ plug-ins, amongst which were the `SIFT stack alignment` plug-in (settings shown in figure 3.1a), the `stackReg` plug-in and the `Rigid Registration` plug-in. None of these had a consistent performance. For example, registration performance was reasonable for the first 25 images, at which point a more complex registration had to be done in which case it failed completely. The image would end up turned for 30 degrees and translated into the upper left corner. All images that would follow were also aligned according to this failed image. Failed registrations were re-done using different parameters in the `SIFT` algorithm, until the results were satisfiable. Whenever the SIFT algorithm would not suffice at all, other plug-ins were used until the registration was satisfiable. Images were cropped again to select an interesting area where a lot of capillaries were present. This last cropping step was necessary as well, since ImageJ uses quite a lot of memory, especially when generating 3D reconstructions. Using an image stack of approximately 1250 by 1250 pixels, 100 images high, ImageJ was quite slow and almost hit the memory limitations. Larger reconstructions will probably be possible when a system with better hardware and considerably more memory is used. The selected area is shown in figure 3.12f. All images could be cropped at once since all images were already aligned. To improve the accuracy of the registration, the images were registered again
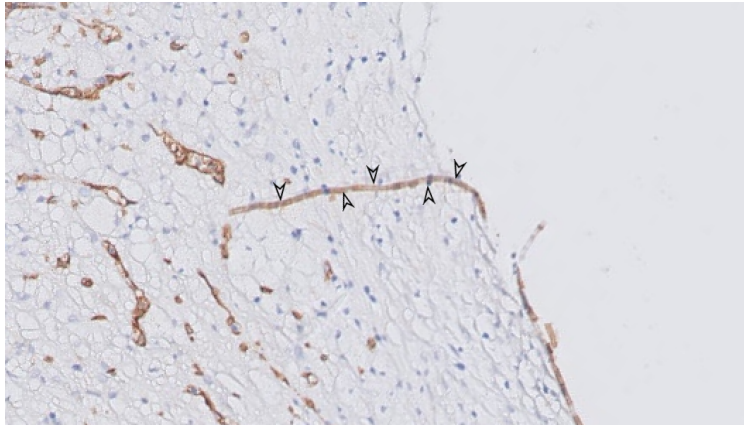
Figure 3.2: Ulex/Hematoxylin slide scan showing damage to the specimen due to the cutting process, indicated by black arrows. This piece of endothelium is clearly torn loose and folded over the intimal tissue.

after the second cropping process. The same work-flow was used as before.

Manual intervention

The images were segmented one image a time, since the images all differed in brightness quite a lot. The fact that the samples contain atherosclerotic regions creates another problem. Because of the 'stickiness' of these fatty regions, the Ulex stain 'sticks' there as well, although there is no endothelium present. In terms of color, this looks almost exactly like the rest of the capillaries and will create quite a large error margin for the final model. Some section images showed this in very little amounts, but others were indistinguishable in terms of color. This is why all these areas have been removed by hand using ImageJ. Though time-consuming, it increased the accuracy enormously.

Other errors that have been manually removed are classification errors due to damaged tissue. These misclassifications arise when a piece of tissue is torn apart, or a piece of endothelium breaks loose. An example of this kind of microtome damage is shown in figure 3.2. Since this piece of tissue is endothelium and stained, the segmentation algorithm will classify it as such. This will generate an erroneous tissue piece in the final model, if not removed manually.

Tissue damage is one of the biggest problems that are related to the reconstruction methods we are using, and hard to prevent with larger specimen. If an area of a slide is missing, it will not show up in the final reconstruction.

Segmentation

After the removal of unwanted regions, segmentation was performed by hand using a color selection method that is included in ImageJ. A typical segmentation setup is shown in figure 3.1b. Using the color threshold values in conjunction with the pre-removal of unwanted areas, the endothelium could be selected without selecting unwanted areas which for example contained fat depositions. The color threshold was optimized for each image

by hand. The segmentation procedure can be improved in the future by using a simple histogram equalization with a histogram of the first image as a reference. This equalizes the colors from all images and might even allow for one single threshold value for all images. Another possible improvement over manual color segmentation is using Ilastik, which will be introduced later on in this document. A third registration cycle was performed after the segmentation. In this case, the `StackReg` plug-in performed better at near-perfect registration than the SIFT algorithm, which seemed to settle with a larger error margin. Both did not perform perfectly, though, so they have been used in conjunction. Whenever `StackReg` failed, the process was interrupted and the SIFT plug-in was used with varying parameters, until the segmentation was near-perfect. A near-perfect segmentation is more important in this case than in the previous, more macro reconstruction of the coronary artery. Not only did the number of slices increase 5 times which increases the chance of an error and causes one error to impact a lot more slides which come after that one, the structures of interest are sometimes only 5-10 pixels in diameter. To be able to create a correct reconstruction, this final registration step has to 'fit' every image as perfect as possible on the previous one. With a set of binary, registered images, an image stack was created in ImageJ and a 3D model was created. Instead of using TDR like in [1], the `3D viewer` ImageJ plug-in was used. The option 'Surface' was used in the menu 'Edit', 'Display as' was used to create a triangulated surface of the created stack. This triangulated model was then exported using File→Export Surfaces→STL (binary). The triangulation methods of TDR are a bit more elaborate and TDR includes some smoothing methods, but since the model was created in ImageJ and the quality of the resulting triangulated model was reasonable, the exportation steps to TDR have not been taken. The triangulated model was imported into Blender where the model was cleaned
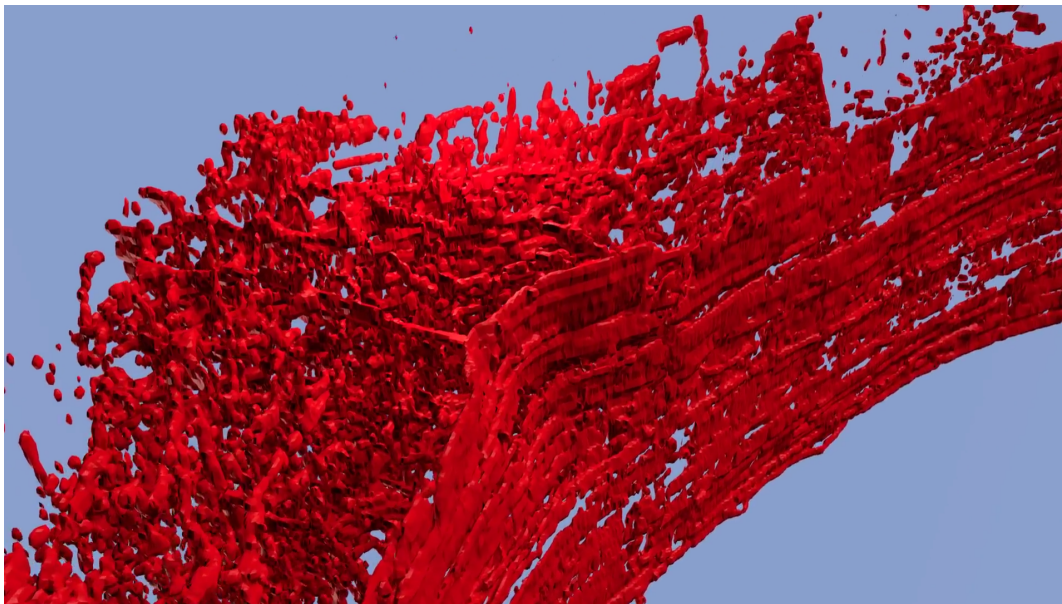

Figure 3.3: Still image from the animation of the reconstruction of capillaries

up (removed unnecessary vertices for better performance) and has been visualized. The final result was an animation [37] where the camera flies through the model to show every aspect of the model. A still image is shown in figure 3.3. The animation has been created because it is impossible to show the 3D relationship of the vast network of capillaries using one snapshot of the model. Using an animation with a moving camera enables the viewer to get an idea of what the 3D network really looks like up close.

Discussion

This 3D reconstruction yields interesting knowledge about the structure of the capillary network. The relationship between the capillaries can be reviewed and properties of capillaries can be calculated such as mean diameter, branching points or even flow analysis of these networks. One interesting feature of these vasa vasorum that can be deducted from this animation is the fact that the supply of the network comes from the inside of the blood vessel. There is a 'pocket'-shape in the lumen which seems to be connected to the network of vasa vasorum to supply it of blood. This is best shown in figure 3.4 and in the corresponding section image of 3.5. In the final model of these 100 section images, 3 such bridges are visible, but this is the only one which is clearly visible in a 2D section image as well. The other bridges can be deducted easily from the 3D model, but are less clear in the corresponding section images. An example of such an intrusion is shown in figure 3.6. This shows that such a 3D visualization can give interesting insights and answers to biological questions, such as where the supply of these vasa vasorum originates from. The quality of the model can still be improved. Some of the slides have been damaged in the cutting process, which is quite common, unfortunately. This means that there can be unconnected points floating in space, which probably should be connected to other tissue. Artifacts like this are nearly inevitable, but during the cutting process with the microtome, extra caution could be taken to prevent damage as much as possible. To improve on this model, "loose parts" could be removed by some algorithm. Moreover, the model output of ImageJ suffers from jagged edges since the algorithm of connecting layer to layer is quite simple. Smoothing might be applied to improve on this.

3.1.2 Overlay

To visualize the location of the capillaries inside the bigger blood-vessel, an overlay has been created using the first Movat stained section image. This image has been added as an image to the scene at the correct position such that it can be visualized in a render. This allows the viewer to understand the location of the capillary network in relation to the peripheral tissue around it. in the final scene, the scanned Movat slide has been registered to fit the Ulex scanned section exactly, after which it has been translated and scaled to the correct position in the 3D scene itself. This method is not perfectly accurate, but it eliminates the need for also rotating the image, which would introduce bigger error margins than this method. An image of this overlay is shown in figure 3.8. The initial goal, in contrary to the overlay of the 2D image that is used now, was to create a reconstruction of the macro-structure of the vessel using Movat stained sections using the same methods as in [1] and overlay this with the capillary model. After the reconstruction of the capillaries, 20 sections of the 100 Ulex stained sections were stained again using Movat's Pentachrome.
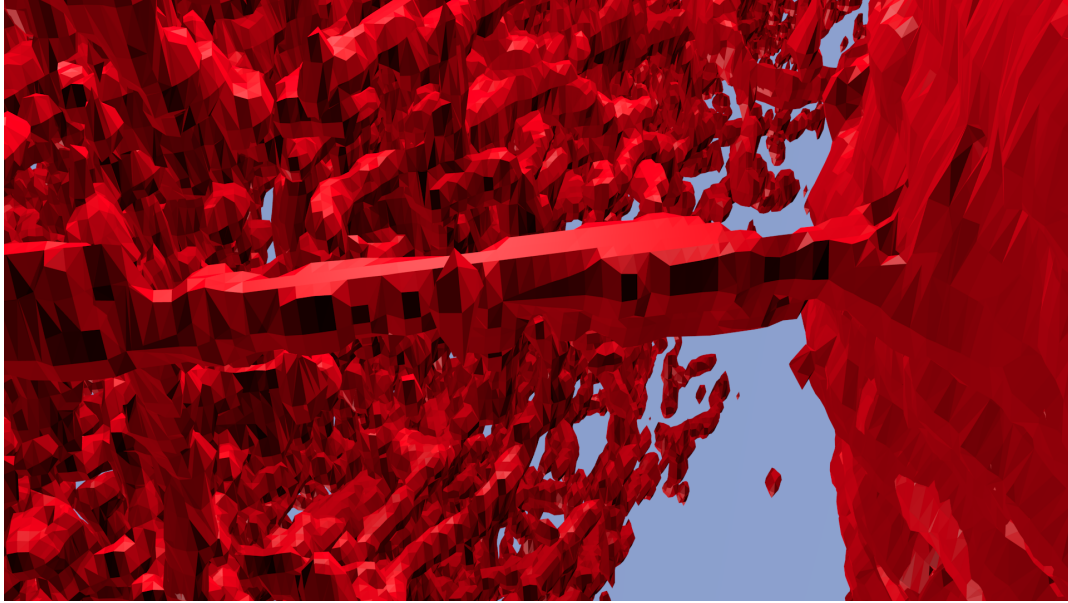
Figure 3.4: Still image from the animation of the reconstruction of the capillaries. This image shows the bridge between the lumen and the inside of the vessel.
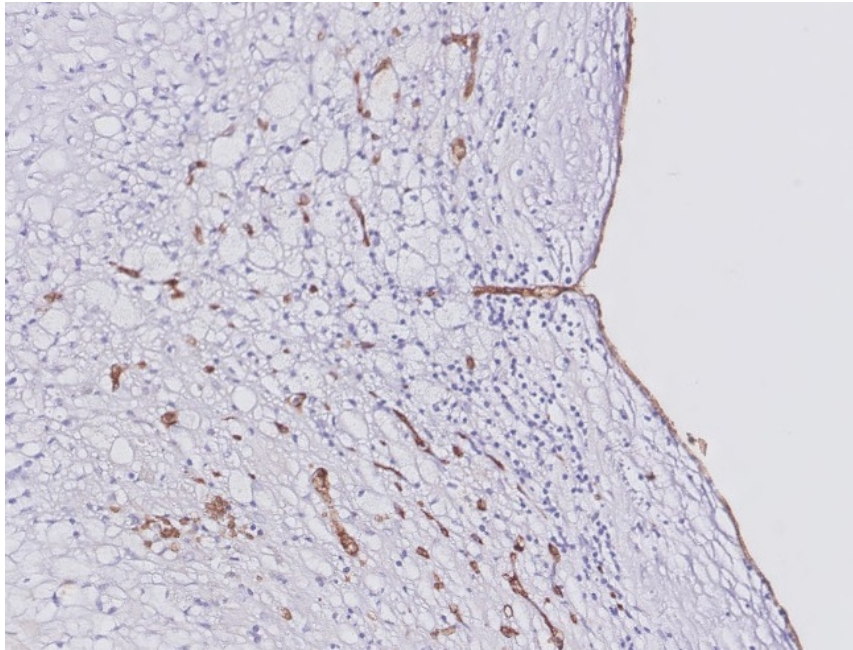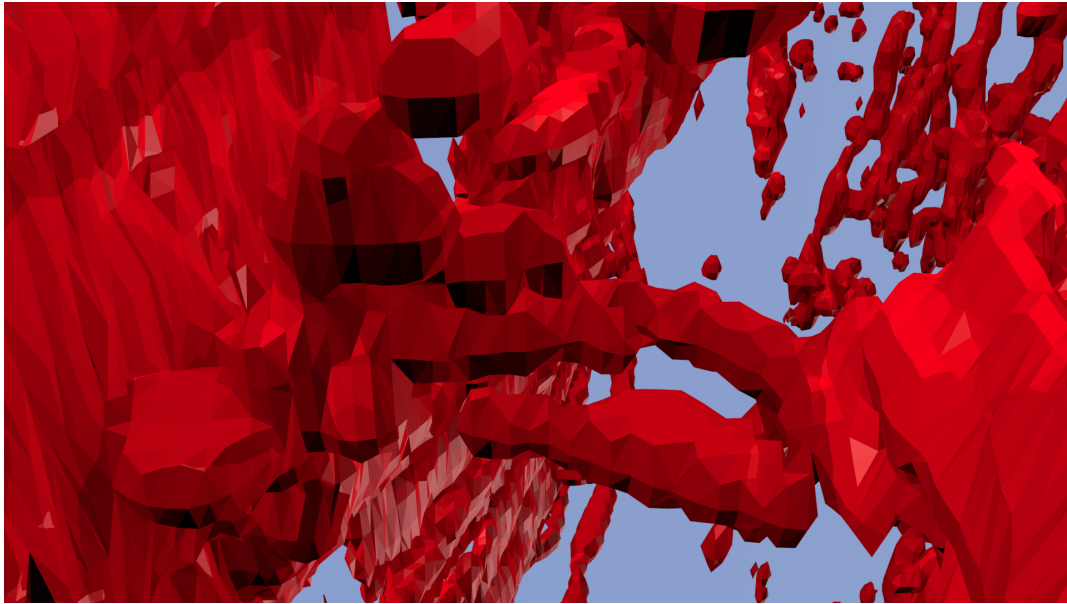

Figure 3.5: Ulex and hematoxylin stained slide scan. Endothelium in **Brown**, nuclei in **blue**. Original tissue originates from a coronary artery, embedded in paraffin. Thickness is 4μm. This particular image contains a significant amount of inflammation cells and vasa vasorum. It also shows an intrusion of a capillary originating from the lumen.

(a) Still from animation
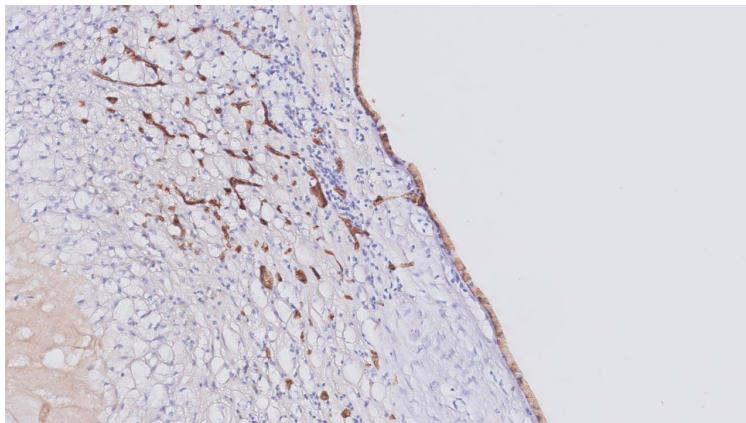
(b) One of the corresponding 2D image

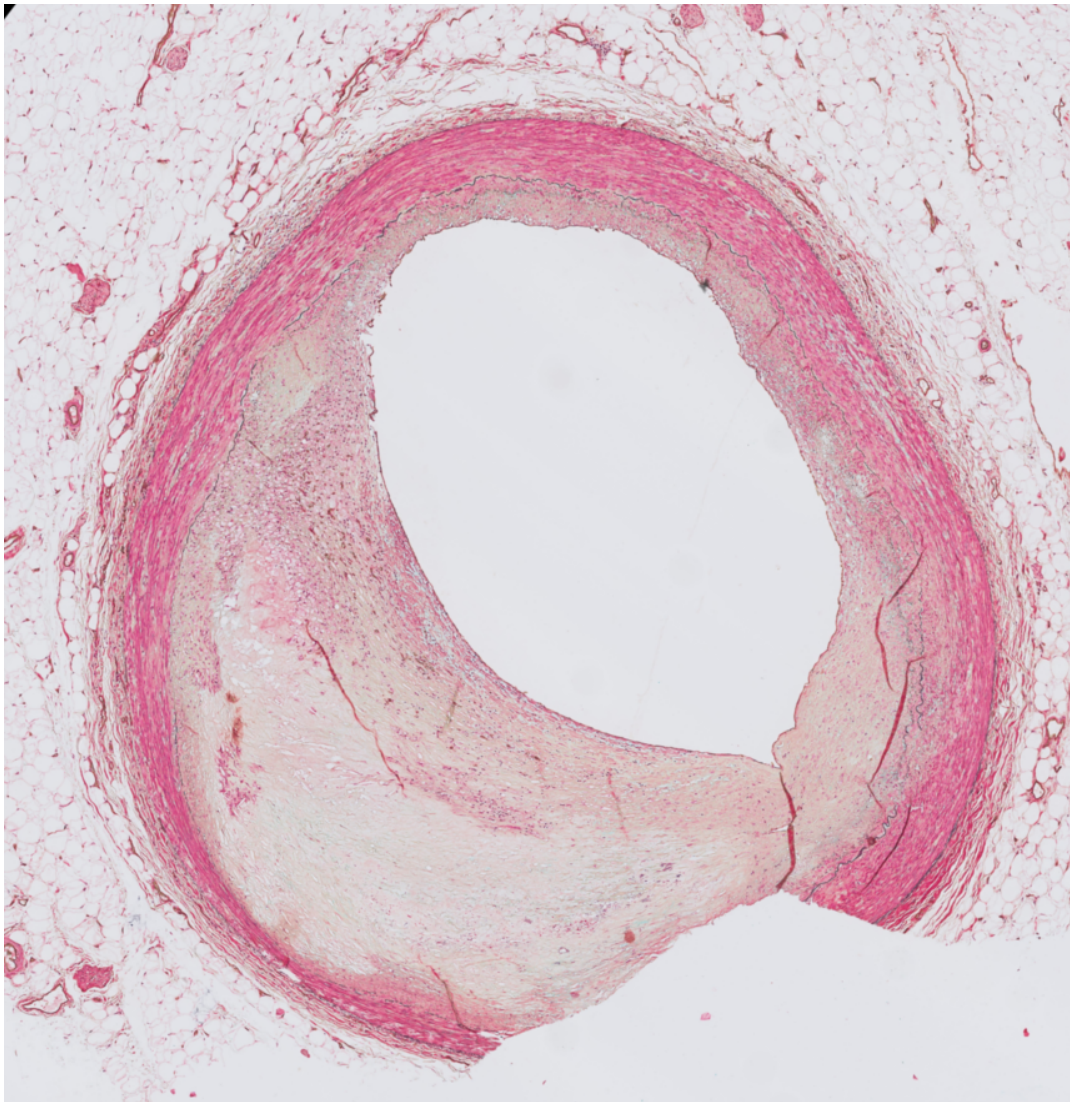Figure 3.6: Example of intrusion which is less clear in 2D than in 3D.

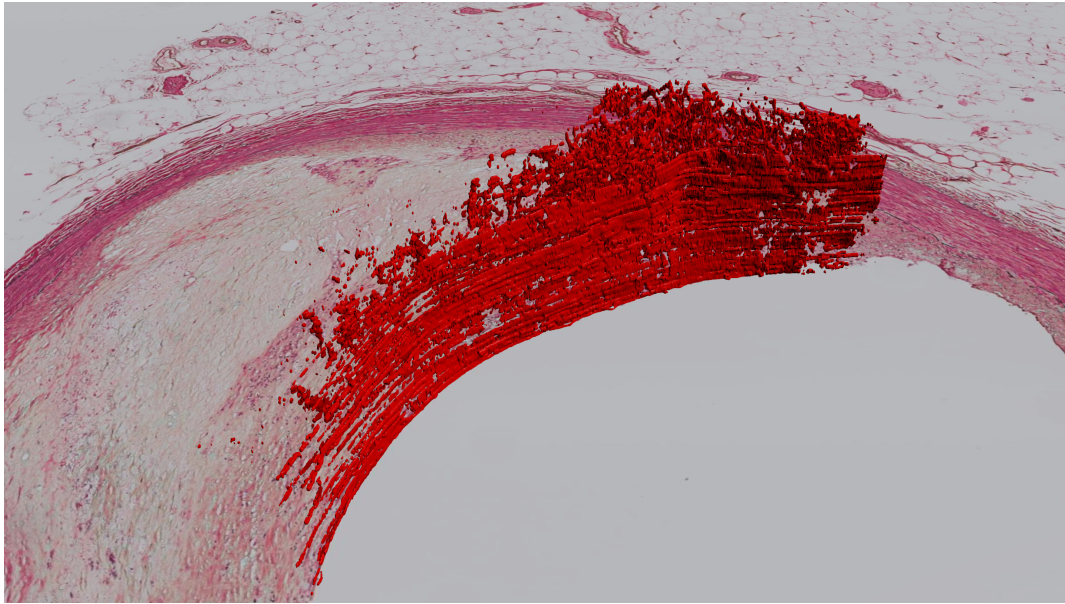Figure 3.7: Ulex stained slide which has been re-stained with Movat.

Figure 3.8: Overlay of Movat re-stained section with the capillary reconstruction.

Instead of an overnight incubation in Xylene, the incubation was done over the weekend. The result was that the proteoglycan stain (normally cyan areas) which normally indicates the atherosclerotic plaque nicely was not really present after staining(image 3.7). The colors of the section image have become quite faint in comparison to other Movat stained section images (figure 2.3). This further complicates the segmentation procedure. To still be able to segment these images automatically, Ilastik instead of the color segmentation methods in Matlab/ImageJ. Ilastik has more elaborate features and uses Gaussian filters and differential filters that help segmenting areas of interest. This allowed for automatic segmentation of the atherosclerotic regions. Since the capillary model was triangulated using ImageJ, so was this model. An overlay has been created as before, but this time every Movat stained section image was registered to it's corresponding original Ulex image to ensure that no rotation was necessary to overlay the two. First, capillaries were segmented in the Movat stained section images using Ilastik. These binary images were registered to the Ulex stained sections perfectly. There was no notable deformation after the re-staining procedure, which made it quite trivial to overlay the two. The registered segmented Ulex section images were then used to register the original Movat section images. Muscle tissue, atherosclerotic regions and the vessel outline were indicated in every image using Ilastik. Since the images were aligned, they could immediately be loaded in ImageJ as an image stack, which in turn could be triangulated into a model, exported as STL file and be positioned in the 3D scene in blender. This positioning also involved a scaling step of 5 times along the Z-axis, since only every 5' slice has been used. The final result is shown in figure 3.10 and 3.11.

The overlay shows us the location of the vasa vasorum in relation to the atherosclerotic plaque. The capillary network is located at the lumen side of the vessel, in between the
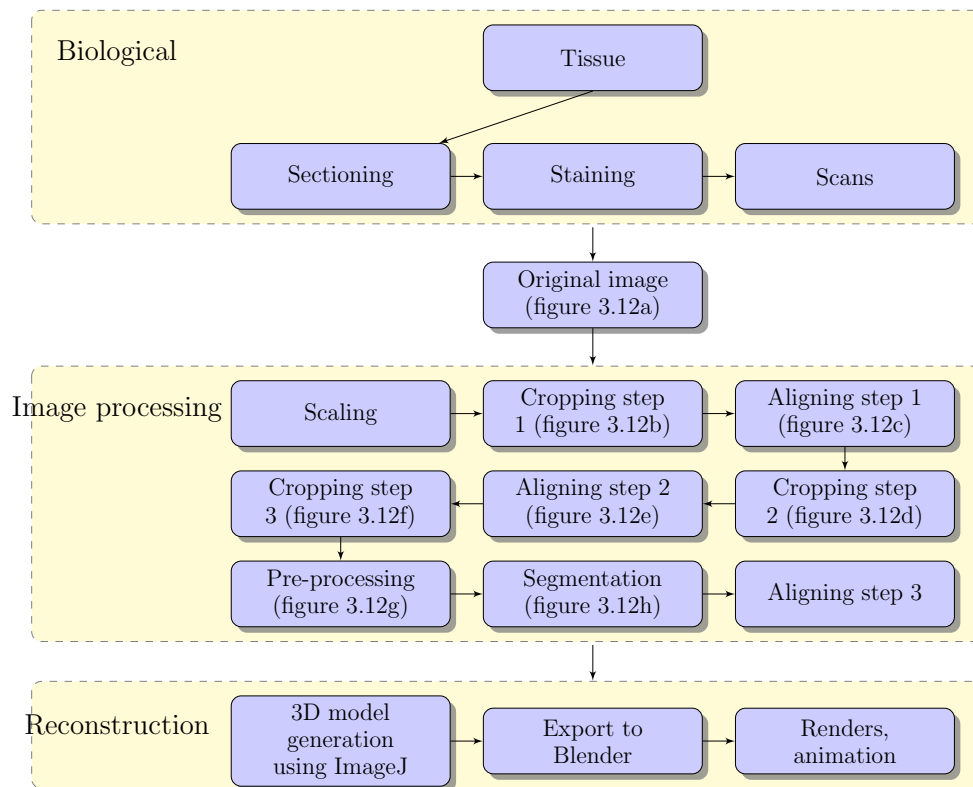
Figure 3.9: Ulex processing pipeline. Schema relates to images shown in figure 3.12.
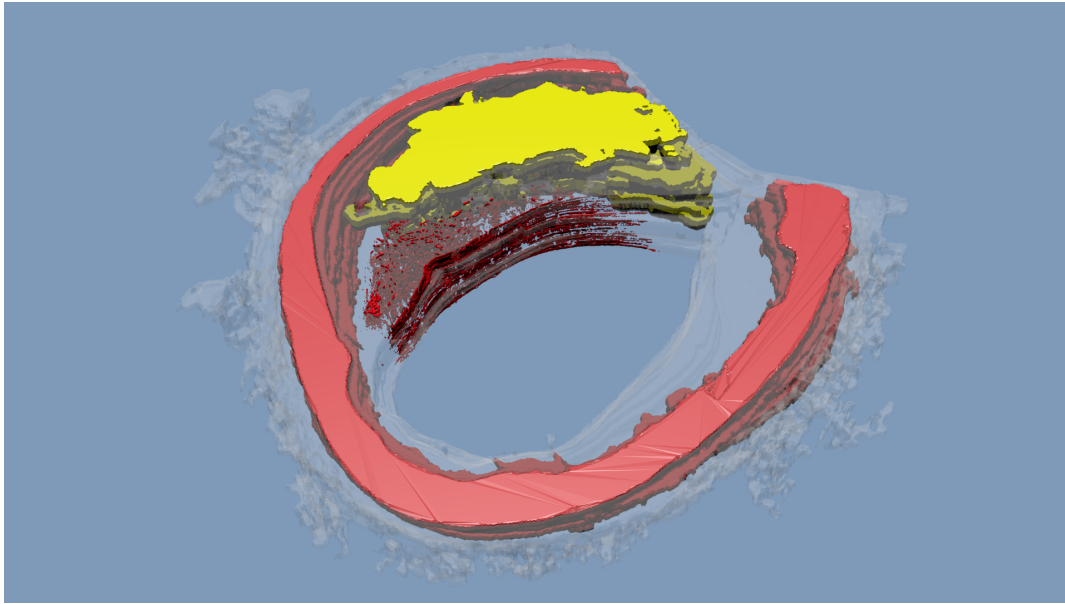
Figure 3.10: Overlay of coronary artery reconstruction combined with the capillary reconstruction. Muscle tissue and capillary network in **Red**, atherosclerotic plaque in **yellow** and in **transparent white** the vessel outline.
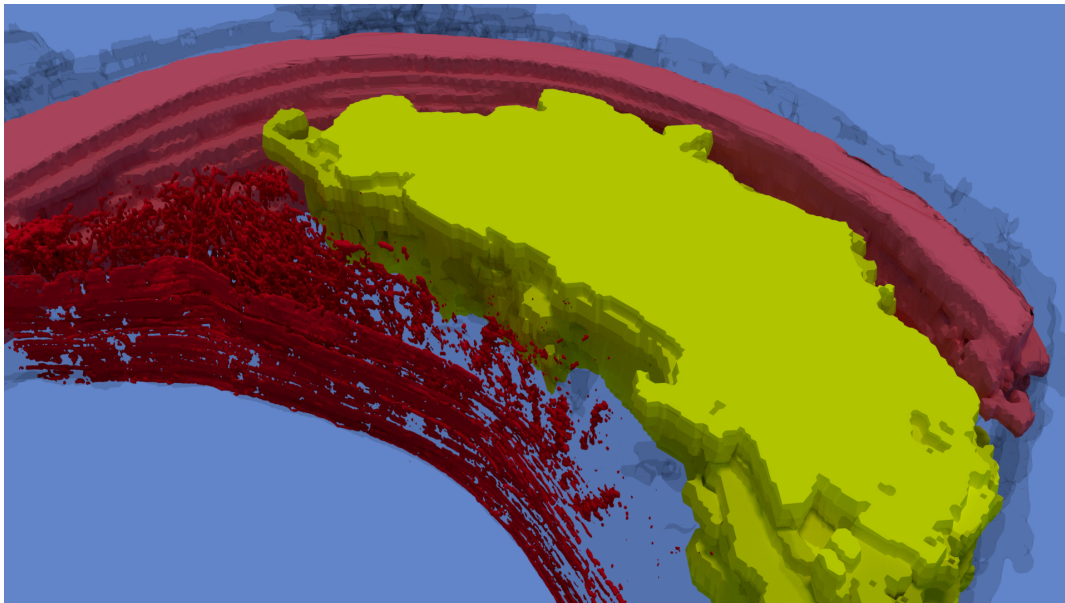

Figure 3.11: Overlay of coronary artery reconstruction combined with the capillary reconstruction. Muscle tissue and capillary network in **Red**, atherosclerotic plaque in **yellow** and in **transparent white** the vessel outline.

(a) Original image

(b) Cropped vessel

(c) Aligned vessel

(d) Cropped vessel

(e) Re-aligned and cropped again

(f) Final cropped vessel

(g) Preprocessed image before segmentation
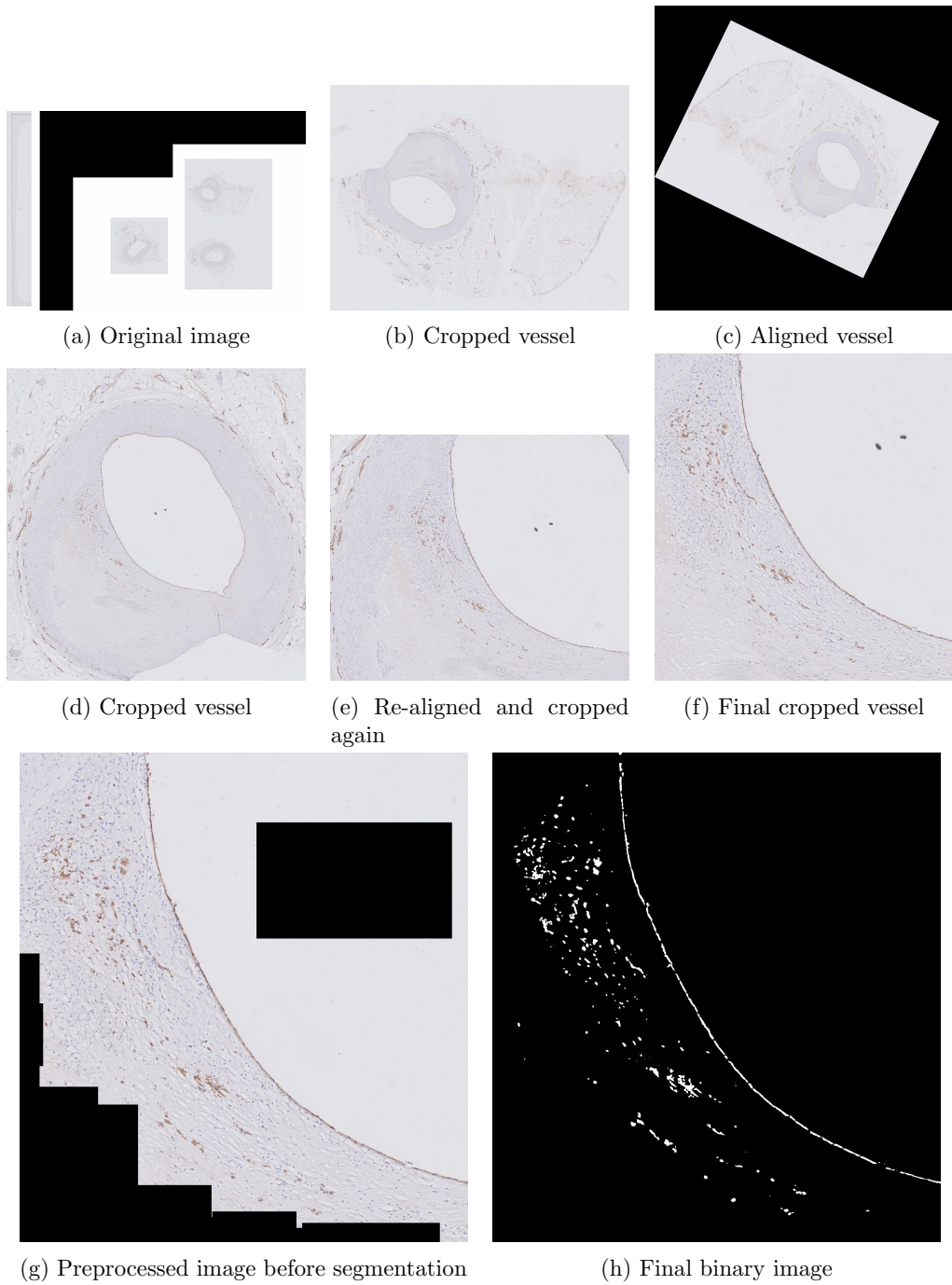
(h) Final binary image

Figure 3.12: Workflow of the processing of Ulex images.

atherosclerotic plaque and the muscle wall. Note that the capillary 3D model is restricted to the selected area in the Ulex section images which was set for performance purposes. A few capillaries continue in the direction of the muscle wall, but the vast majority of capillaries are shown in the final model. A bigger model which ranges over the complete Ulex model would be considerably more complex, since a lot more deformation will occur on such a large scale. Rigid registration tools as those which are used in this project will not suffice. This would yield a more complete biological picture which can be more informative than this current model. In the future, such a capillary reconstruction could be created using more than 100 slices. The model that is shown only has a height of 400 μm. Increasing the height of the reconstruction will give a better overview of the vessel. Using the same methods as discussed above, it should be possible to add at least 100 extra slices. It might be necessary to use a machine with more than 16 GB of RAM.

3.2 Bicuspid Aortic Valve disease

The second investigation in this thesis was aimed at determining defects in the arterial wall of BAV patients. Since structural differences show up in the structural filaments which have a very complex, micro-structure, this fits in the description of the micro-scale problem, since the structures that are the subject of investigation are smaller than a micrometer. To investigate the pathological processes of the dilation of the wall of the coronary artery, this project aimed to create a 3D reconstruction of aortic tissue from BAV patients. This section describes the process of investigation, imaging and analysis of the gathered data.

3.2.1 Pilot

The first idea was to create a 3D stack conform the methods of the atherosclerotic reconstructions. Tissue was cut in slices of 4μ thickness each, stained with Sirius red and scanned in using the PHILIPS scanner. This pilot contained 20 consecutive section images. An example section image is shown in figure 3.13. These sections were reconstructed using the same work-flow as before. As a start, the red-stained collagen fibers were chosen as a segmentation target, where the yellow muscle fibers following second. This might give insight in the 3D organization of the fibers.

A range of 20 consecutive sections has been aligned and a stack has been created using these sections. The resulting stack is shown in figure 3.14. However, information gained using this method unfortunately informs only about the macro-relationship of the vessel. The 3D relationship of the fibers did not become quite clear using a reconstruction like this. The amount of sections is relatively small and could be increased, but the reason for the failing of this reconstruction is the distance between slices. 4μ is too thick for a section if the goal is to reconstruct the 3D structure of the fibers. Sections could theoretically be cut at smaller thicknesses like 1 μ, but deformation problems will grow and damage to slices will occur more often. Lower thickness than 1 μ are not feasible.

The initial goal was to use the same methods as for the reconstruction of the capillaries, but the slight deformation that occurs when using paraffin slices, in combination with the low Z resolution that comes with the use of physical sections made these methods not
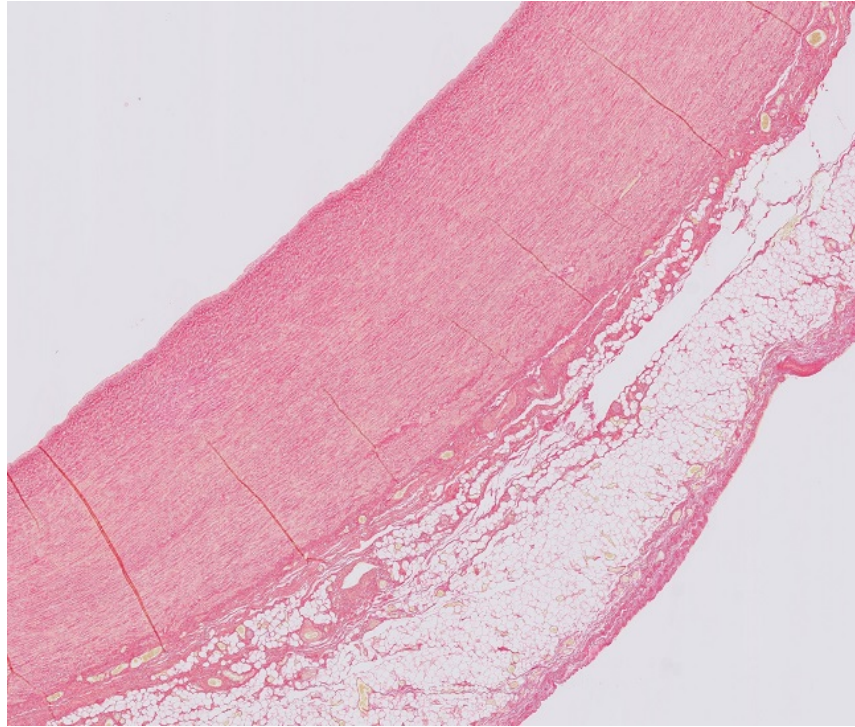
Figure 3.13: Sirius red stained section (4μ) which was used to create a 3D stack to look at the 3D relationship of fibers
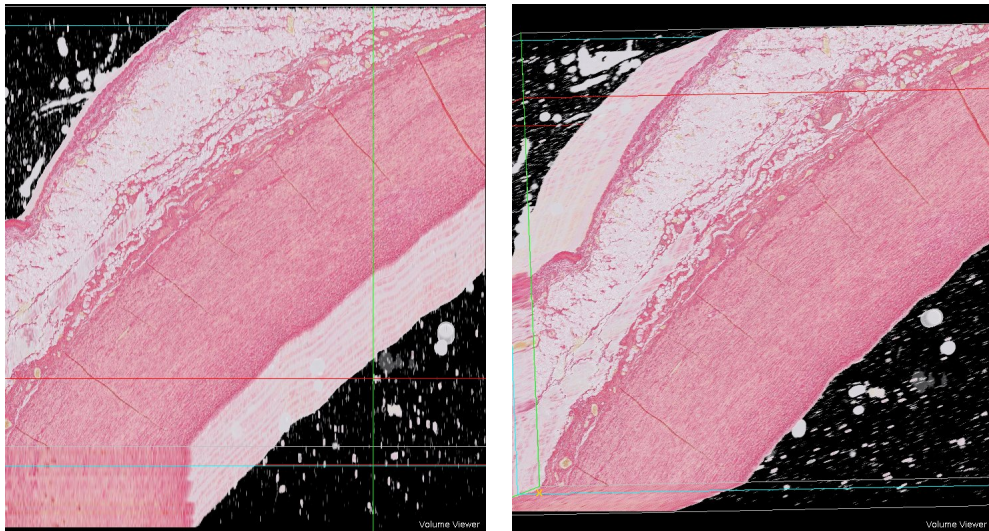

Figure 3.14: Stack of Sirius Red stained sections.

unsuitable. In previous cases deformation posed a challenge for registration, for example in the capillary reconstruction case, but the structures that were the target of reconstruction were larger than the muscle fibers we have been looking into for the BAV problem. Using the extremely high resolution output of the PHILIPS scanner, we can actually get into a lot of detail with an individual section. Other advantages in respect to other imaging methods are the fact that color information is available as well and the overview that is achieved using such a microscopic scanner. However, since the fibers are only distinguishable at the highest of resolutions, the smallest amount of deformation would introduce enormous error margins in the 3D reconstruction. Not only that, as it becomes clear that if we are looking at a structure so small, the wide-field microscope which is used to scan these slides becomes a serious bottleneck since it is scanning the whole of the 4μ sections. Apart from that, segmentation is a difficult problem at such a scale. The problem lies in the fact that though stained red, the fibers are sometimes very thin and it is hard to reach high accuracies using the methods we have used before. It is difficult to exactly describe what parts should be selected and which parts should not. This pilot demonstrated the need for a different approach when the subject of investigation is at μm scale. The methods used before do not apply in this case.

To counteract the above-mentioned problems, we decided to use confocal microscopy. This has a few clear advantages as it can create a focal plane which solves a range of problems immediately. Registration is not needed anymore since the tissue that is scanned in has a certain thickness which is scanned layer for layer, preserving the X-Y alignment. Also, we are not looking at sections 'from the top', looking at the whole thickness of the section, but at one layer of the specimen at a time. This allows for reviewing the 3D-relationship of the fibers in greater detail. Deformation between different layers of one stack will not occur anymore since there are no physical sections anymore. Moreover, segmentation is no longer a problem that has to be solved using software. Using biological principles and the principles of fluorescence, we can specifically stain certain structures, while others can be seen using autofluorescence. This enables us to get intensity values for each filament instead of a binary segmentation.

There are disadvantages to report as well, as confocal microscopy only allows us to review a very small portion of tissue and takes a long time to scan an image.

3.2.2   Imaging

The first stacks were captured with a confocal microscope using sections that were stained using Sirius Red, according to [22]. Available samples originated from previous studies and ranged in thickness from 4-50μm. After staining, slides were covered using Pertex mounting medium. One of the first stacks that was created is shown in figure 3.15. This image shows a clear difference between the collagen and elastin fibers. Image stacks like this would be suitable as input for a model, but the goal was set to include actin fibers in the model as well.

To include actin in the model, Phalloidin was used. At first, phalloidin was tested using a newly cut paraffin section which was stained with phalloidin-647. The results are shown in figure 3.16.

The phalloidin signal was very weak and as a result, the gain and the laser were increased far beyond normal levels. This automatically has a noisy signal as a result. The
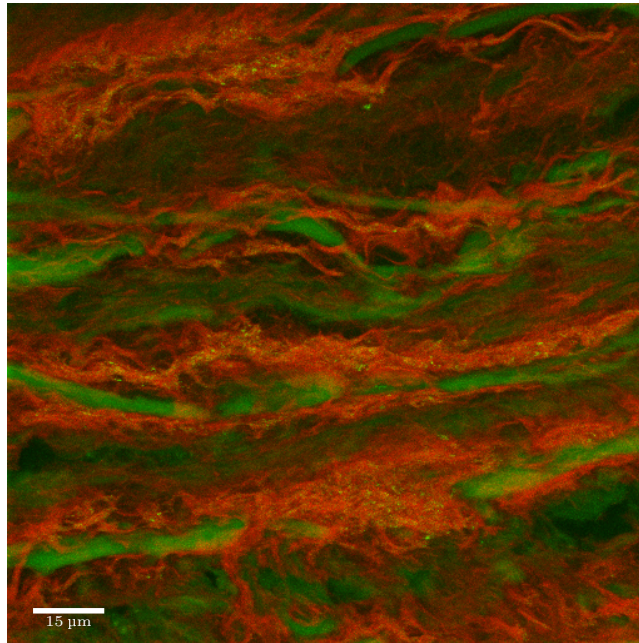
Figure 3.15: Max projection of a confocal microscopic image of a 20μ section aortic tissue stained with Sirius Red. The red channel represents collagen (excitation 543nm), the green channel represents elastin (excitation 488nm).

(a) 543nm excitation (b) Elastin channel (488nm excitation) (c) Actin channel (633nm excitation)
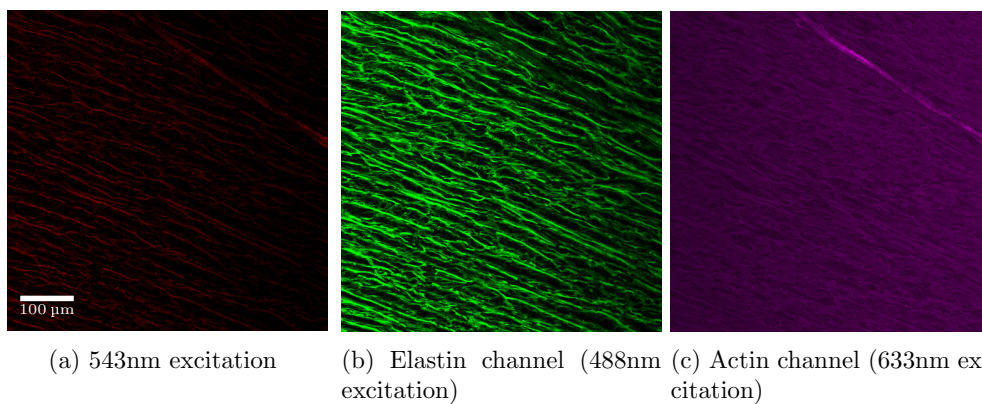
Figure 3.16: Confocal microscope image of a paraffin slide of aortic tissue stained using Phalloidin. Magnification is 10x. Note that the 543nm channel is an empty control.

(a) 543nm channel(red) and elastin(green)   (b) Elastin(green) and phalloidin(purple)
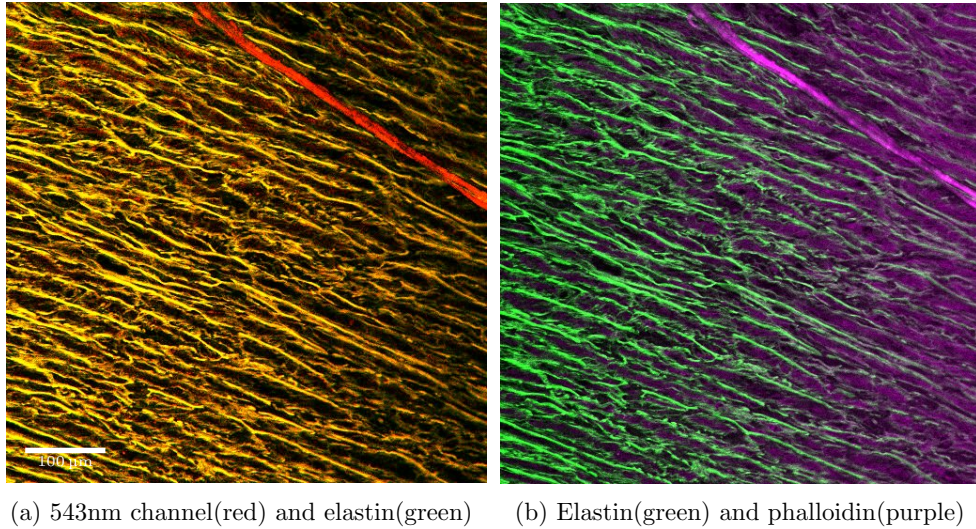
Figure 3.17: Visual co-localization analysis of confocal image of aortic tissue stained using Phalloidin.

collagen channel contains a very weak bleed-through signal of elastin. Note that this was as expected since we applied no Sirius red nor any other collagen-stain. The overlay of both channels in figure 3.17 shows the strong co-localization of the elastin and 543nm channel and the phalloidin channel compared to the elastin channel. According to this image, the collagen and elastin channels were exactly the same. The phalloidin channel was clearly different, however has some co-location with the elastin channel and the signal was quite weak and thus the output image was noisy.

To create an image that includes all target structures, phalloidin was applied after the Sirius red staining. A new paraffin section was cut, stained with Sirius Red and on top of that, Phalloidin-647 was used, what meant that there should be 3 fluorescent channels which were excited at 488, 543 and 633 nm, respectively. Phalloidin incubation was shortened to half an hour instead of 45 minutes because Sirius red washes off in the aqueous circumstances of the phalloidin incubation. The results are shown in figure 3.18.

The actin signal was still weak and noisy, and co-located with the collagen and elastin channels. One of the reasons for this observation could be an interaction with Sirius Red. This stain is quite a rough stain with various acids that are used in the process, which might interact with actin or phalloidin in such a way that it does not bind successfully. To improve on the actin channel, we decided to switch to a multi-photon confocal laser microscope. Using a microscope like this, collagen can be visualized using Second Harmonic Generation(SHG) [38, 39], such that the Sirius red stain would not be necessary anymore. This technique relies on the chirality of the collagen molecules, which will excite when using a wavelength of 800 nm. This enables us to view the collagen without staining it first, which would eliminate any effects of Sirius on the actin channel. Elastin is also visible when excited with 800 nm at the same time. The multi-photon microscope is coupled with a detector with three channels which can capture a certain range of wavelengths independent of each other.
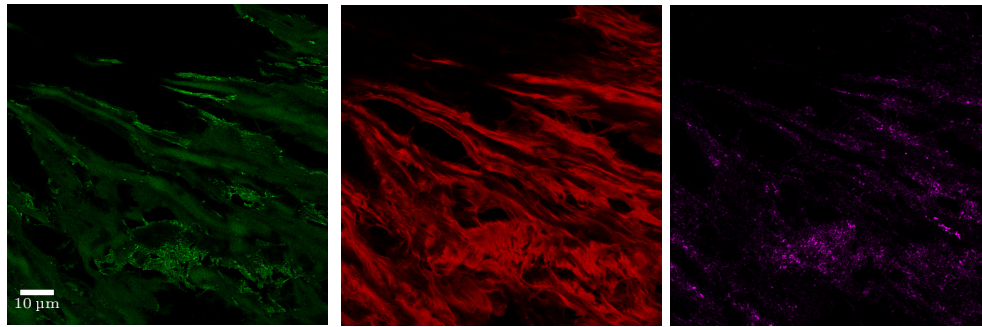
(a) Elastin channel (488 nm)   (b) Collagen channel (543nm)   (c) Actin channel (633nm)
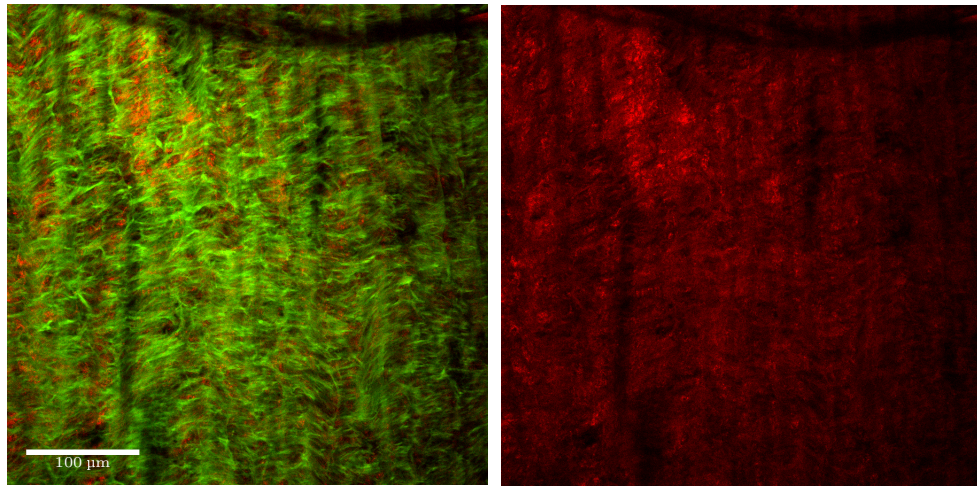
Figure 3.18: Confocal microscope image of paraffin slide of aortic tissue stained using Sirius red and Phalloidin-647.

A new paraffin section was cut and stained with phalloidin. Results are shown in figure 3.19. The detector range was set at 371-425nm for the first channel, and 473-532nm for the second channel. The laser power was set to 20%. Note that the collagen channel in figure 3.19b has quite a weak signal. This image has been contrast stretched to visualize the filaments better, and the detector gain has been increased far beyond normal levels, which resulted in a noisy image.

Since the collagen channel showed less signal than expected when compared to Sirius red, we decided to use another mounting medium. The reason for this is that SHG of collagen relies on the chirality of collagen, which could possibly be destroyed by xylene. Up until this point, we have used Pertex as a mounting medium, which contains xylene. During the embedding and fixation procedures for paraffin, xylene is used as well. At this point, we have experienced a technical problem with the microscope, which could also be the cause of the previous results concerning the SHG of collagen. After setting up the laser at 800nm, overall signal quality was quite bad. When this value was changed to 810nm in this case and even back to 800nm, the problem was gone and the signal strength was reasonable. The exact reason for this failure is unknown. To prevent problems regarding the mounting medium, we did not mount the material at all and kept the specimen in a PBS buffer. This lead to an image that is shown in figure 3.20.

This image shows that the collagen channel did not show a very consistent signal compared to the collagen channel of the Sirius red channel, although it was stronger than it was in figure 3.19. We have also combined this with the use of phalloidin, which could potentially give an image with all three target structures. The resulting image is shown in figure 3.21.

The actin channel was excited using the 633 nm laser. The actin channel is shown again in figure 3.21b where it has been contrast stretched. The signal quality of the collagen channel and the actin channel was not very high. Another observation was that the actin channel signal was mostly gone after the use of the 800nm laser. This is best visualized in figure 3.21c. The darker lower part of the image has just been excited with the 800nm laser. To create this image, the 633nm laser has been used before the 800nm laser was used to avoid losing signal. Although this seems a case of radiation damage, this kind of damage

(a) Collagen channel(red) and elastin(green).　　　(b) Collagen channel

Figure 3.19: Multi-photon confocal microscope microscope images of tissue, excitation at 800nm and detector ranges at 371-425 and 473-532nm.
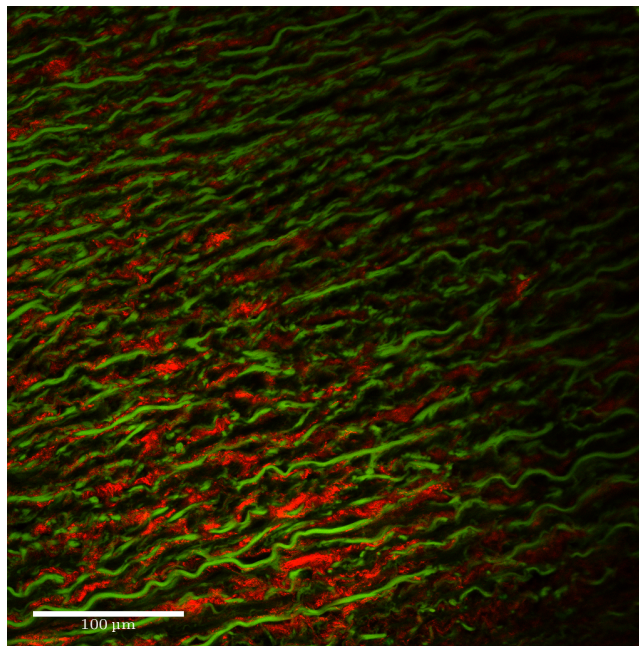

Figure 3.20: Multi-photon confocal microscope image created using a paraffin section, stored in PBS. No mounting medium used. Collagen in red, elastin in green. Excitation at 800nm, detector ranges at 371-425nm for collagen and 473-532nm for elastin.

(a) Combination of three channels, collagen in red, elastin in green and actin in purple.

(b) Actin channel alone

(c) Example of tissue fixation damage to the actin channel after use of multi-photon laser

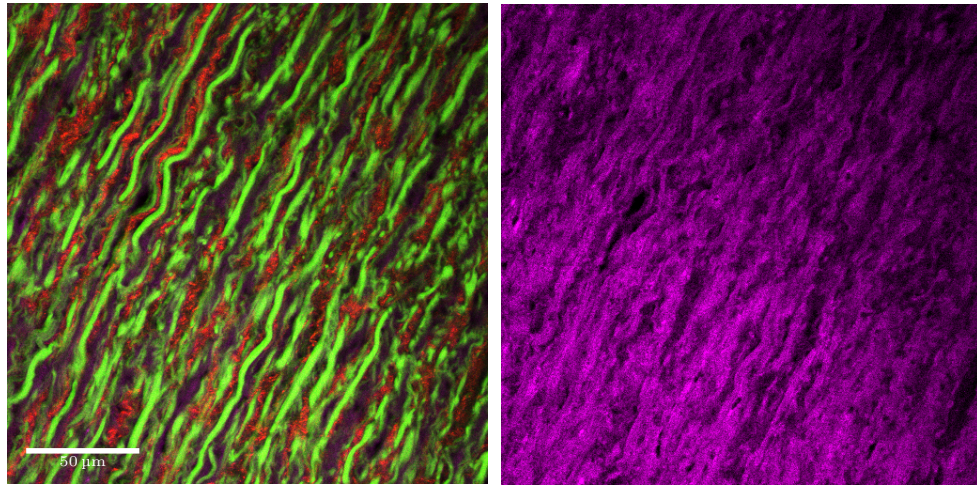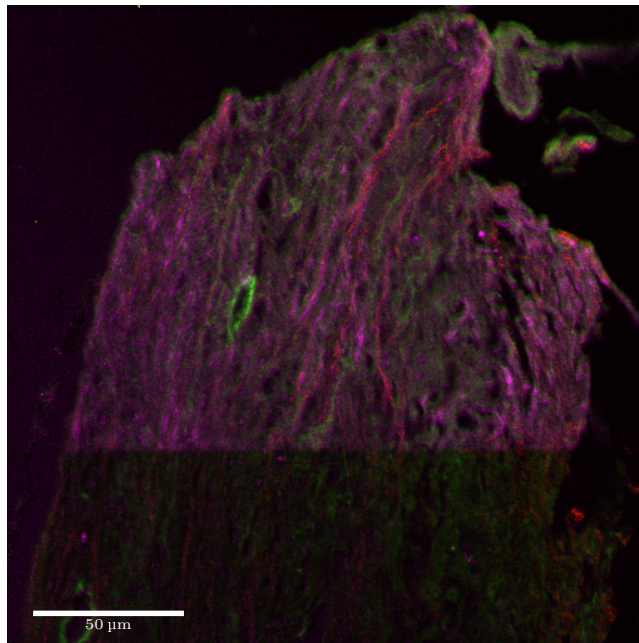Figure 3.21: Multi-photon confocal microscope images of paraffin-embedded tissue. Excitation at 800nm and detector ranges at 371-425 and 473-532nm. Phalloidin was excited at 633 nm before the use of the 800nm laser. No mounting medium used.
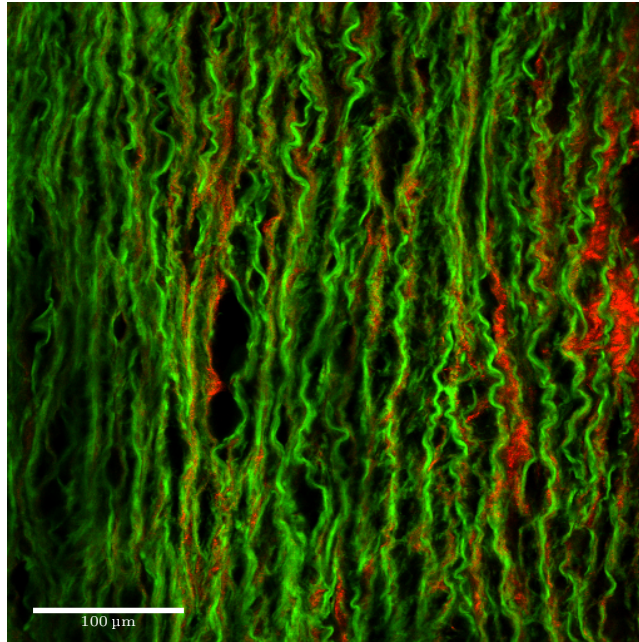
Figure 3.22: Image created using a frozen section, stored in PBS. No mounting medium used. Collagen in red, elastin in green. Image was captured using a multi-photon confocal microscope, with excitation at 810nm, detector ranges at 371-425nm for collagen and 473-532nm for elastin.

is very uncommon when using a two-photon laser, since these kind of lasers use a high wavelength which means that the light has low energy. This means that radiation damage is less likely to occur. A more plausible explanation would be that this phenomenon is caused by the fixation process which interacts with structures in the specimen. Up until this point, paraffin-embedded tissue was used and the signal strength of the actin channel has remained faint and thus noisy. It seems that the mounting medium and/or the fixation process not only effects the collagen's SHG signal, but the phalloidin signal as well. It was suggested that the weakness of the actin channel signal might be related to the use of paraffin, more specifically to the fixation techniques that have been used, as they are known to cancel out a lot of signal when using phalloidin since the fixation steps might interact with the cytoskeleton. Even using unstained paraffin sections and using only PBS as a medium for imaging, the phalloidin signal was weak.

To improve on the general signal quality including collagen and actin, we have tried to use snap-frozen sections instead of paraffin. Using snap-frozen sections, any contact with Xylene will be prevented and hopefully the amount of generated signal will increase. Frozen sections have been used from earlier studies. For a first experiment, unstained sections were used and excited using the multi-photon laser scanning microscope to image for collagen(SHG) and elastin. The results are shown in figure 3.22. This image shows that the collagen channel locally shows better signal using frozen tissue, but using the Sirius red images as a reference, we do see that this is more local collagen than we would expect.
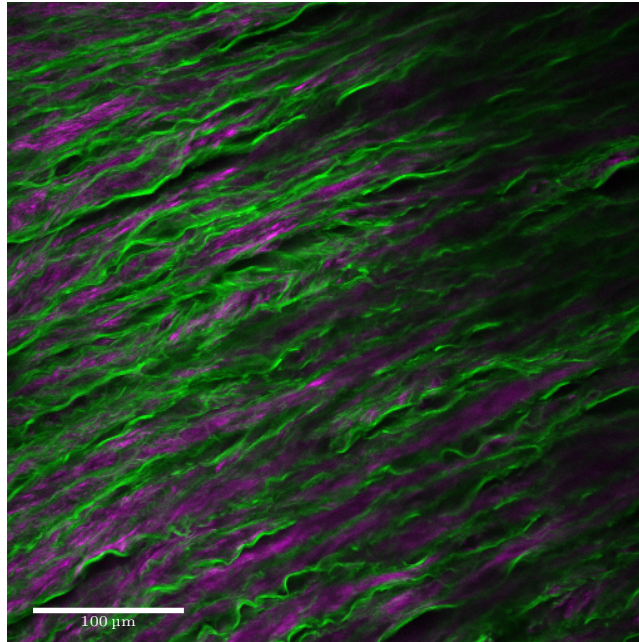
Figure 3.23: Image created using a frozen section, stored in PBS. No mounting medium used. Actin in Magenta, elastin in green. Excitation for elastin autofluorescence at 488 nm, excitation for phalloidin at 633 nm.

A possible explanation could be that only a particular type of collagen shows up using SHG. Specifically staining collagen using Sirius red might improve this signal. Another explanation could be that Sirius red is not specific to collagen, but stains actin as well. This would mean that it might be even better to use SHG instead of Sirius red, because Sirius red would not be specific enough and probably effects other stains. To investigate whether the actin signal is better using frozen sections instead of paraffin sections, we used another frozen section and applied phalloidin. For imaging, we used the 488 laser and the 633 to avoid the use of the multi-photon laser, since this laser seems to not always improve the signal quality. This resulted in figure 3.23.

This image shows a much clearer result in the actin channel than before. The signal to noise ration was considerably higher, and the detector gain could be kept within reasonable limits while still producing a quite strong signal. This shows that the actin channel improves if the use of xylene is prevented. After this initial test, actin and collagen have been combined into one image by using the 800nm laser to excite the collagen using SHG. Results are shown in figure 3.24. Though the image shows better signal for all channels compared to any of the unstained paraffin sections imaged until now, staining with Sirius red seemed to yield a more solid collagen signal than SHG techniques. Only parts of the collagen within the imaging region are visible using SHG. Compared to the Sirius red signal, which may be less specific to collagen, it produces a quite local signal. Lastly, to improve on the collagen channel, we have tried to use Sirius red in combination with phalloidin like before, but now use it on a frozen section instead of a paraffin-stained
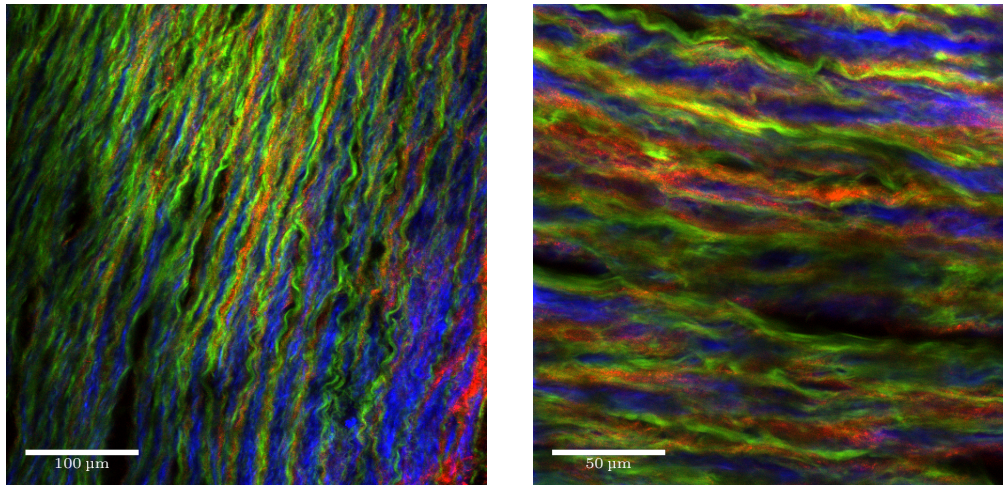
(a) Combination of three channels, collagen in red, elastin in green and actin in blue.

(b) Combination of three channels, collagen in red, elastin in green and actin in blue. Zoomed in 3 times.

Figure 3.24: Multi-photon confocal microscope images of frozen tissue, stained with phalloidin. Excitation at 800nm and detector ranges at 371-425 for collagen (SHG) and 473-532nm for elastin. Phalloidin was excited at 633 nm.

section. This might give better actin results than before because we suspect that paraffin has negative effects on phalloidin. The results are shown in figure 3.25. This figure shows that Sirius red has a strange effect on phalloidin, as suddenly in the phalloidin channel there is an overlap with both elastin and collagen channels, while in the control section that is stained only with phalloidin, the actin channel does not co-locate with elastin at all. Actin antibodies have also been used in an attempt to increase signal strength and specificity. The results of these experiments are shown in figure 3.26. The antibodies showed less filaments than phalloidin when comparing figure 3.23 to figure 3.26a, showing that it might be more specific to certain kinds of collagen than phalloidin. The antibodies also show overlap with the collagen channel when used in combination with Sirius red (image 3.26b), which indicates that Sirius red not only shows up as collagen when excited with a 563 laser, but co-locates with actin as well.

The complete imaging search has been summarized in table 3.2. It can be deducted from this table that none of the configurations we have tried so far show a reasonable signal for both elastin, actin and collagen whilst also being available in larger quantities. Since time was running out, we have decided to revert back to only staining the tissue with Sirius red, without capturing any actin at all. The reason for this is that the staining procedures of Sirius Red are quite straightforward, the collagen signal is quite strong, and the combination with elastin works well. The best solution in terms of imaging result would be to use frozen sections and stain these with phalloidin. This however requires the tissue to be snap-frozen in the operating chambers, which would require a few extra weeks to collect. Paraffin tissue blocks are available in larger quantities as they have been gathered over the years into a database.
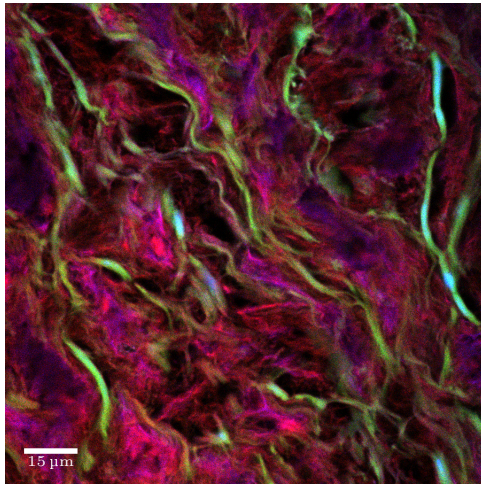
(a) Frozen section stained with Sirius red and phalloidin. Collagen in red, elastin in green and actin in blue.
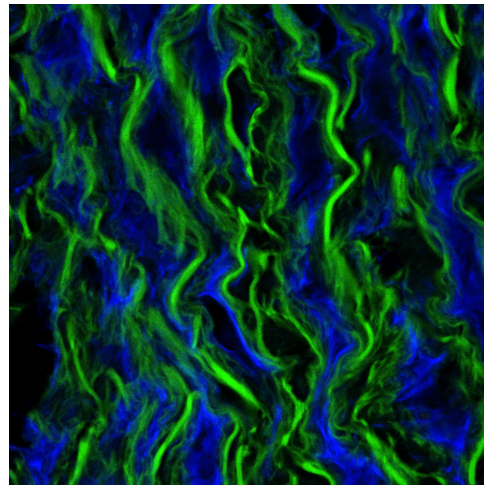
(b) Frozen control section stained with phalloidin. Actin in blue, elastin in green.

Figure 3.25: Confocal microscope images of frozen tissue. Tissue is stained with Phalloidin and Sirius red. Excitation at 568 nm for collagen, 488 for elastin. Phalloidin was excited at 633 nm.
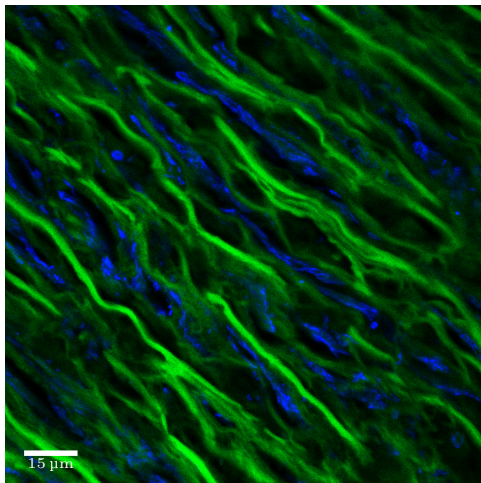
(a) Frozen section stained using an actin-antibody. Elastin in green and actin in blue.
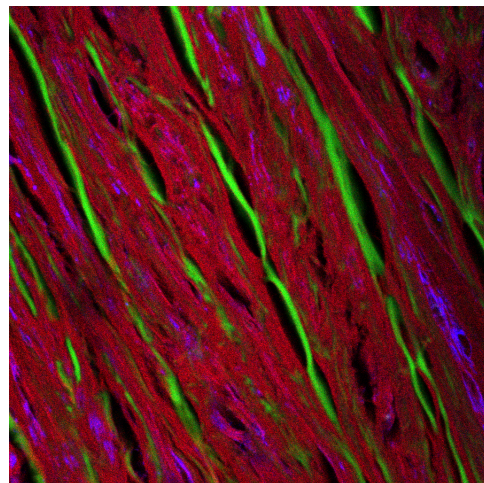
(b) Frozen section stained with Sirius red and an actin-antibody. Actin in blue, elastin in green and collagen in red. Excitation at 568 nm for collagen, 488 for elastin. The antibody was excited at 633 nm.

Figure 3.26: Confocal microscope images of tissue. Test with frozen sections stained with Sirius red and/or Phalloidin

Table 3.2: Imaging overview. 'vis.' means visualization. A '∼' means that the results were considered not adequate.

Slice type		Collagen vis.		Actin vis.		Mounting		Channels			Availability
Paraffin	Frozen	Sirius red	SHG	Phalloidin	Antibody	Pertex	PBS	Elastin	Collagen	Actin	
✓		✓				✓		✓	✓		✓
✓				✓		✓		✓	X	∼	✓
✓		✓		✓		✓		✓	✓	∼	✓
✓			✓			✓		✓	∼		✓
✓			✓	✓			✓	✓	✓		✓
✓			✓				✓	✓	✓	∼	✓
	✓			✓			✓	✓	✓		∼
	✓			✓			✓	✓	X	✓	∼
	✓		✓	✓			✓	✓	✓	✓	∼
✓		✓			✓		✓	✓	✓	∼	✓

Table 3.3: Research groups

#	Type	No. of patients
1	Tricuspid normal	5
2	Tricuspid dilated	5
3	Bicuspid normal	4
4	Bicuspid dilated	5

3.2.3 Analysis

Tissue was used originating from 19 different patients. Patients were selected from 4 different groups which are listed in table 3.3. The only group which did not contain 5 patients is the BAV normal group, since this group is quite rare in the database. Using these groups, we hoped to be able to review differences between the tissue of patients who suffered from a dilated aorta and patients who did not, as well as compare patients with a bicuspid aortic valve who developed a dilated aorta to those that were a-symptomatic. From every single patient we reviewed multiple sections during the project, mainly to improve on the staining method. For the final investigation, only one section has been used per patient. The final sections had a thickness of 4μ. 3 confocal image stacks were captured from the media per patient, as well as one from the adventitia. All images have two channels, which contain collagen and elastin. As discussed in the previous section, all sections were stained using Sirius Red. XY resolution was 1024x1024 pixels, the mean number of layers was 10 and the optical layer thickness was set to 0.5μm. Examples are shown in figure 3.27.

At first, the samples have been evaluated visually. This evaluation yielded no solid conclusion. Elastin fibers are the most distinguishable of the two, and further investigation into the structure of these teaches us that most elastin fibers have a curved, wavy shape, but can contain some irregularities, even in healthy controls like in figure 3.27. No significant differences were observed in comparison with tissue of BAV patients with a normal aorta. Even so, there might be an abnormality present which is too faint to be spotted with the naked eye. To evaluate the differences between the tissue samples, data mining methods have been used. If data-mining methods are able to make a consequent distinction between the two different tissue samples, this might indicate that there is a significant difference between the tissue samples of BAV and normal tissue. On the other hand, if image recognition methods give no results whatsoever, this might indicate that there is no difference at all and the problem might be elsewhere. Prior to data-mining, feature sets must be made. The first approach that we used was the creation of 'handcrafted' features. These features are listed in table 3.4. With these features, we have tried to describe the properties of the shape of elastin fibers and the collagen matrix. The second approach was to use more established methods in the field of image recognition which have been applied successfully in the past, for example Local binary patterns(LBP) features [40] and Histogram of the Oriented Gradient(HOG) features [41]. The main advantage of hand-crafted features over these two is whenever there is a significant difference found between two groups of samples, we can find out exactly which of the features contributes most to this difference, which might be a lead for the issues related to BAV disease. A disadvantage could be that these features do not contain the exact information that is needed to
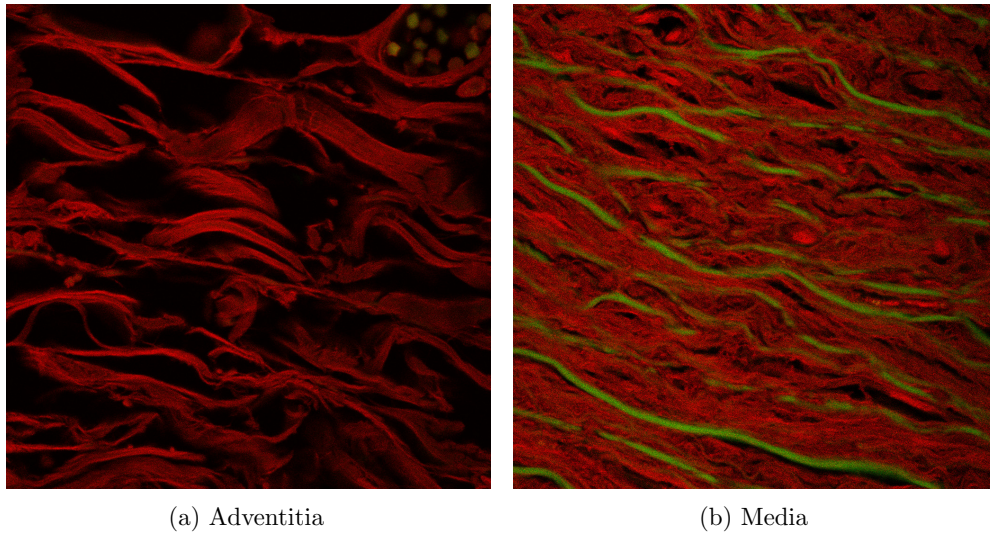
(a) Adventitia

(b) Media

Figure 3.27: Final images of tissue samples. Healthy control with tricuspid valve, normal width aorta. Elastin in green, collagen in red. Highest intensity layer is shown here.

Table 3.4: List of handcrafted features generated for the final microscopy images

1	Length of elastin fibers
2	3D Convexity
3	Thickness of Fibers
4	Number of fibers in image
5	Mean size of fiber
6	Percentage of collagen
7	Percentage of elastin
8	Ratio of collagen/elastin
9	Number of 'holes' in collagen matrix
10	Directionality of elastin fibers

distinguish between different classes, which means that even if there would be a difference, we would miss it.

After generating a feature set based on table 3.4, using the code that is shown in appendix A listing 1, a range of models has been used to predict the class of every image. Every image has been classified using the classes that are listed in table 3.3. An example of a 3D stack for elastin is shown in figure 3.28. This stack also shows that there is little spatial information available if 4μm slices are used, in combination with a cover slip which compresses the tissue as well. The handcrafted set of features contains 3D descriptors, the generated LBP features are taken from the highest intensity layer. The models were validated using leave-one-out(LOO) cross-validation, which means that all data from one patient was left out at a time, after which the rest of the data was used to train the model, which in turn was used to predict the class one patient that was left out. Using this method, one can determine whether the model is performing well on data
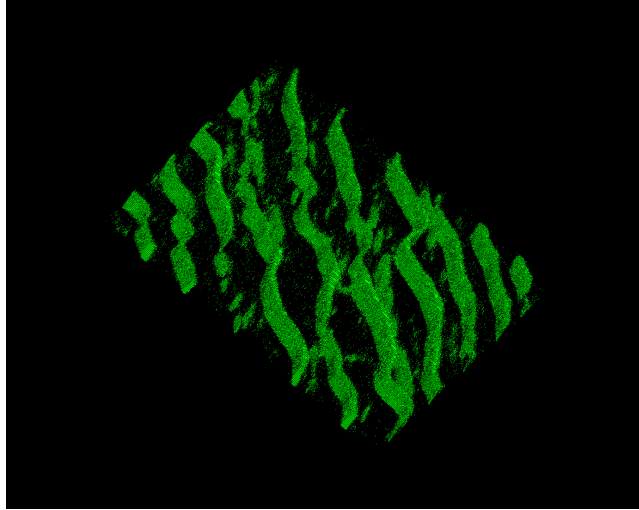
Figure 3.28: Elastin stack visualization. Captured using the Zen software suite.

Table 3.5: List of algorithms that were used to predict different classes of tissue.

1	Decision tree
2	Adaboost classifier
3	Random forests
4	Support Vector Machine
4	Linear Support vector classifier
5	ExtraTrees classifier

it has never seen, such as to prevent overfitting. This way we can guarantee that the model has predictive value, instead of just explaining the variance between the different images. The algorithms that were used are listed in table 3.5. These algorithms are all algorithms capable of predicting classes, since we are dealing with a class-prediction problem. All these algorithms are part of the Sci-kit learn package for Python [29]. To compare the performance of these algorithms, we have used them all to predict the class of the samples using the LOO cross-validation. To test, 100 runs were done where the dataset was randomly split into train/test for every run. Results of this initial prediction are shown in figure 3.29.

RandomForests showed best performance on the test set with an average score of 0.30. The RandomForest algorithm is known to be able to handle overfitting quite well, although the score on the training set was 0.98. The scores of all algorithms all were a little bit better than random (0.25 in this case), but SVC performed worse at 0.21 on average. Pre-processing steps have been used, in particular a standard scaler and a dimensionality reduction. Both of these are part of the sklearn package.

As is shown in figure 3.30, using only 3 components for the dimensionality reduction makes that the prediction results were a bit better than before with an average score of 0.29 and a highest score of 0.31 for AdaBoost and ExtraTrees, suddenly. This shows that pre-processing is a valuable tool when dealing with a small amount of data to predict a
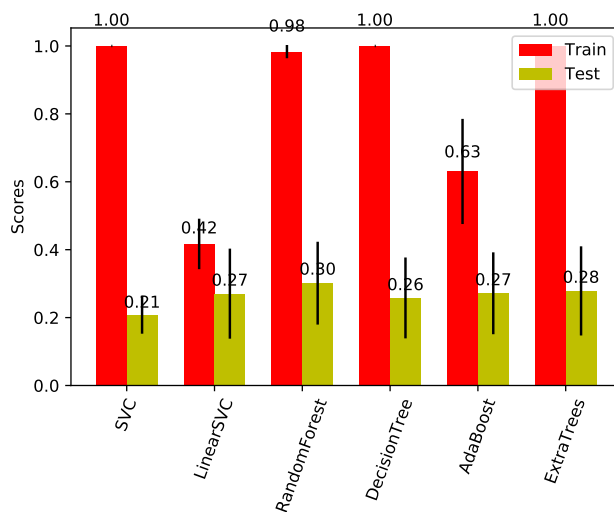
Figure 3.29: Prediction results using handcrafted features. No pre-processing. Results generated using 100 random runs per algorithm.
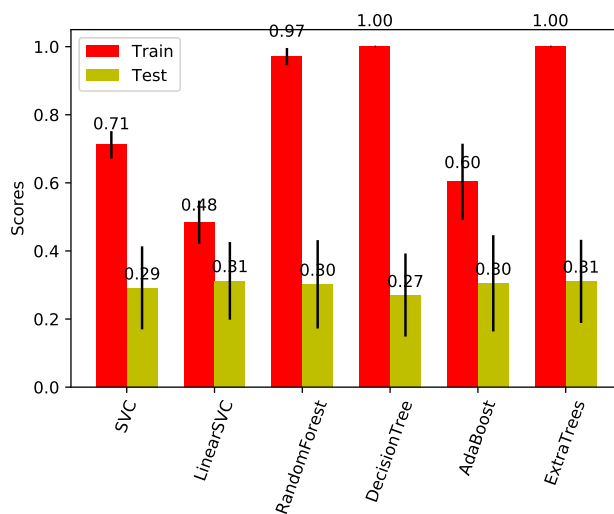

Figure 3.30: Prediction results using handcrafted features. Pre-processing steps taken, 3 components selected for the dimensionality reduction. Results generated using 100 random runs per algorithm.
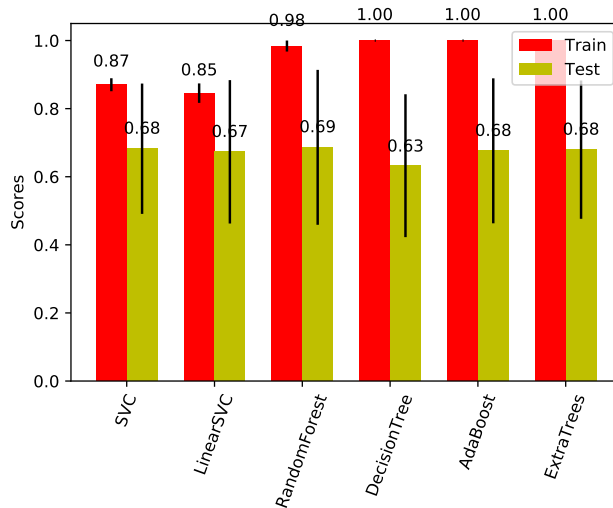
Figure 3.31: Prediction results using handcrafted features. Pre-processing using 5 components. Results generated using 100 random runs per algorithm. Only distinguishing between bicuspid and tricuspid valve.

class. Even though the scores improved, 0.30 is a very low score since it is just above random. This means that neither of the algorithms have a significant predictive value based on the features that we have generated during this project. To be able to verify this even more, we have tried to simplify the resulting model by only using 2 classes instead of 4 by eliminating the dilated/non-dilated classes and test the predictive abilities again.

Figure 3.31 shows the results of this prediction. The results are significantly better, but this is only logical since the amount of classes was divided by two. Even so, scores of 0.70 are reasonably good in comparison with the 0.30 that we saw earlier.

None of the algorithms seemed to have a solid predictive ability using the features that we have been using. This might indicate that there is no real difference, but to increase the certainty of this statement, we have used more established image descriptors as LBP and HOG features as well. LBP features and HOG features have been generated to describe these images. The LBP P and R variables were set to 8 and 2, resp. The images were rescaled to 1/8th of the original size for performance reasons. Configurations using higher resolutions have been tested as well, but there was no significant improvement on the results. The output was a feature vector of the same size as the image which will be 128x128 after the scale operation. This vector of 16,384 is too large and not very informative as well since every single pixel and its surroundings is transformed into a feature, which gives very limited, very local data unless combined in a bigger feature. The local binary patterns are usually accumulated in a histogram which has length P+2. Since the P variable is 8, the histogram has a size of 10 in this case. Examples of such a histogram are shown in figure 3.32.

Using these LBP features, we hoped to improve the prediction results in regard to the previous scores of the handcrafted features. We have used the same data-mining algorithms to perform the analysis. The results are shown in figure 3.33. The results

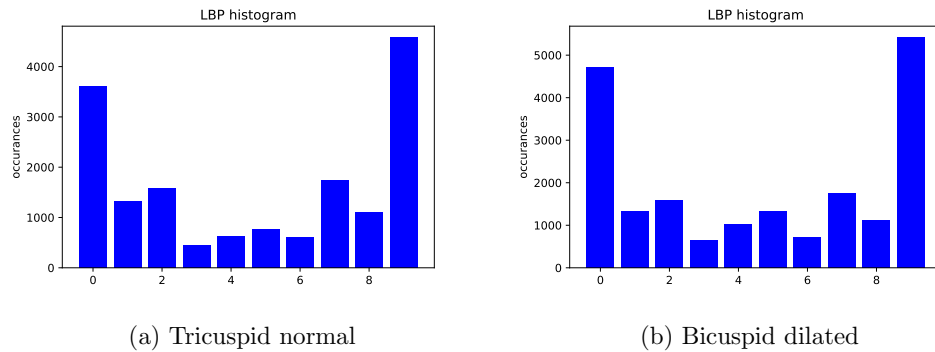(a) Tricuspid normal   (b) Bicuspid dilated

Figure 3.32: LBP histograms of images of the elastin channel.

are comparable with the handcrafted runs in terms of scores, except for the fact that the ExtraTrees classifier works better in combination with preprocessing, resulting in a score of 0.34. These scores are slightly higher than the handcrafted scores, but not adequate.

We have also investigated whether we were able to distinguish between bi- and tricuspid aorta's only, using the LBP features we have used before. Results of this investigation are shown in figure 3.34.

The highest scoring combination was a pre-processing step using 5 components in conjunction with an SVC, which scored 0.69 on average. To try to improve more on this previously used method, we have used HOG features in conjunction with LBP features. We hoped that this combination would increase the prediction capabilities of the model. Results are shown in figure 3.35. We have only looked at the differences between bi- and tricuspid patients.

The results show that there is no increase in predictive ability. AdaBoost and LinearSVC seem to perform better using the HOG features as well, but the highest performance is lower in comparison with the LBP only case. Even using the LBP and HOG features, prediction results did not indicate that there was a consistent difference between the two research groups. Low scores can be interpreted in two ways. Low scores can indicate that there cannot be made a solid distinction between the two groups on the basis of the features that we have generated, but it can also mean that there is no difference between the tissues of these groups. Dilated and non-dilated groups have also been compared using these methods, but the average test-set prediction scores were even worse than random with a highest average score of 0.47. To try to verify the methods on validity, we have used the same methods on a different example than the BAV investigation.

3.2.4 Verification

We have tried to verify the methods that we have used during the analysis of the microscopic images. To do so, we have used the methods to predict whether a certain image was taken from the adventitial regions or the medial layer of the blood vessel wall. The area where most of the images were taken of is the media, but for every patient, one image stack was also captured from the adventitial regions. These images are easily distinguishable by the naked eye (see figure 3.27). This was a base-line test to verify that the methods would
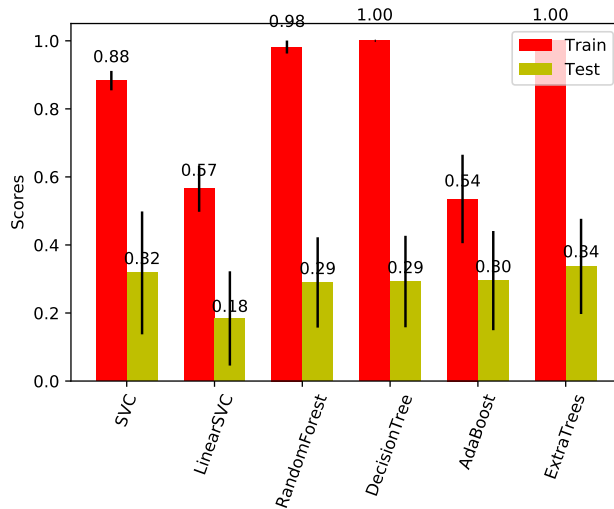
Figure 3.33: Prediction results using LBP features. Pre-processing using 5 components. Results generated using 100 random runs per algorithm.
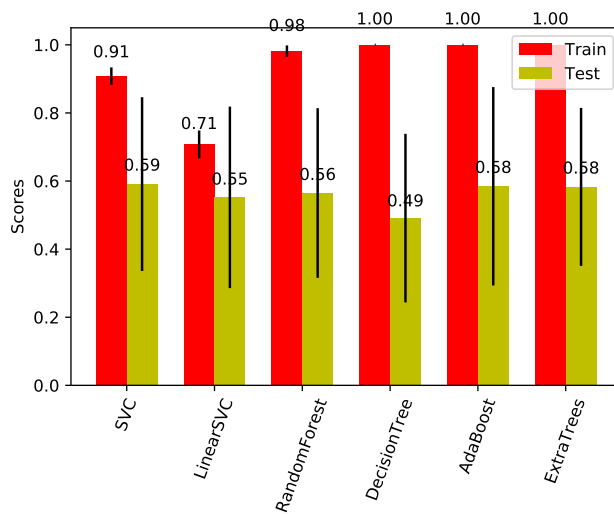

Figure 3.34: Prediction results using LBP features. Pre-processing using 5 components. Results generated using 100 random runs per algorithm. Only distinguishing between bicuspid and tricuspid valve.
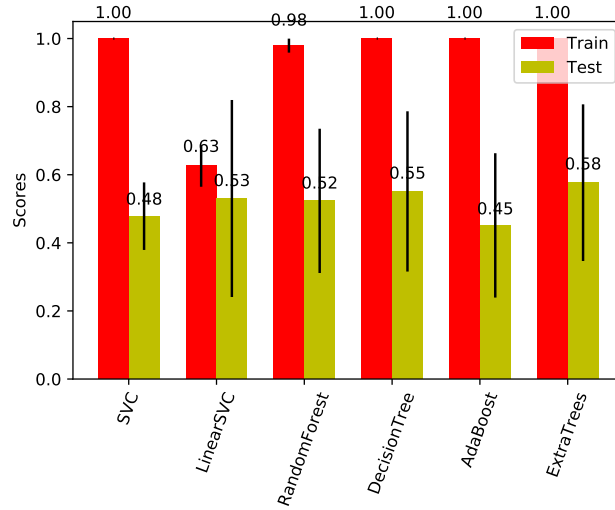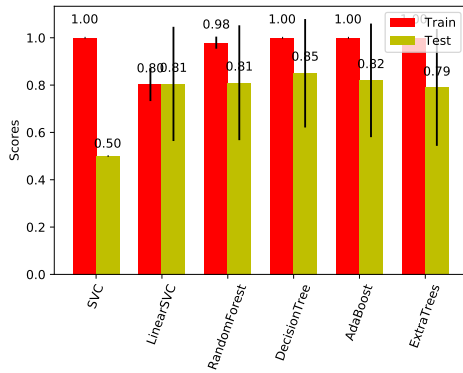
Figure 3.35: Prediction results using LBP and HOG features. Pre-processing using 5 components. Results generated using 100 random runs per algorithm. Only distinguishing between bicuspid and tricuspid valve.

work in simple cases. Results of this comparison are shown in figure 3.36. This figure shows that higher scores are obtained when using classifiers for a simpler problem, where peak average test result performance is around 0.90. These results are generated using an LOO evaluation, using one patient per time as a test set, and randomly selecting one of the three medial images in conjunction with the single image of the adventitial layer. This means that if the algorithm guesses randomly every single time, the score would be around 0.50.

To further investigate into the predictive abilities of these algorithms, we have used tissue from Marfan patients as well. The downside to this comparison is that all Marfan tissue we used was snap-frozen, which might have different morphology compared to the paraffin sections. Most of the Marfan slides were not stained as well which means that they have been compared to slides stained with the Sirius Red stain, which might have an impact on the strength of the elastin channels as well. LBP features have been generated based on the elastin channels only, since this was the only channel that was present in all Marfan section images. Results are shown in figure 3.37, which shows that the highest score for predicting Marfan's syndrome based on the elastin channel is 0.95 which is a combination of a linearSVC and LBP features.

These verifications show that using a method like LBP in conjunction with an SVC could be a suitable method to detect differences between tissue samples. Even so, using these methods on the four patient groups that we have yielded no solid differentiation between classes, not even when split up in subtasks like comparing only the bicuspid to the tricuspid group or dilated versus normal aortic tissue.

The predictive ability of the models used might increase with the number of microscopic images that are used. Five images per class is a relatively small dataset for the complex data that images are. Algorithms like those we used benefit from a lot of data. Every

(a) Handcrafted features results
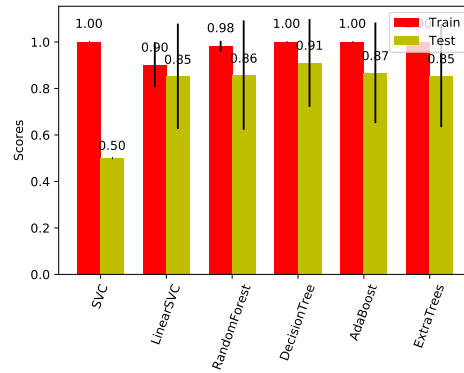
(b) LBP features results

Figure 3.36: Results of predicting the region of the blood vessel (adventitial versus medial layer). No pre-processing steps taken.
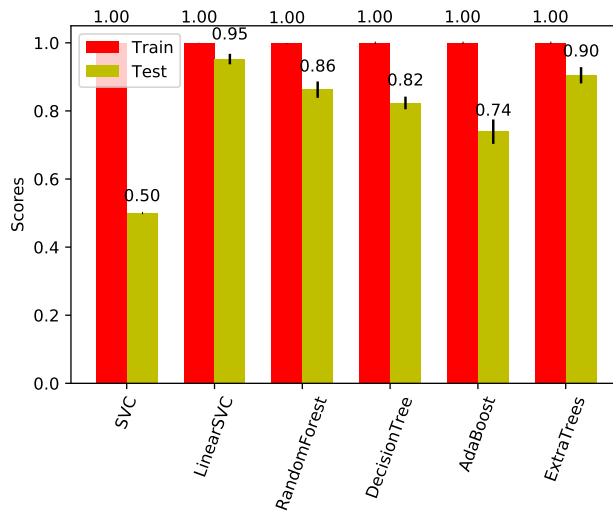
Figure 3.37: Prediction results using LBP features generated using elastin channel. No pre-processing. Predicting whether patient was a Marfan's patient.

data-mining problem deals with a certain amount of variance. Right now, the variance is just too large compared to the size of the dataset to be able to work with it. As this project was only a first impression, the dataset size was quite small. If the amount of data were to be increased, the slight differences that might be present can be detected and analyzed. These analysis steps are not really useful at this point, since the models have not proven to be good enough to differentiate between the classes. Also, for the LBP feature analysis, only 2D images have been used for the analysis. the slides that were used were only 4 μm thick, so the gain of 3D data would have been quite minimal. In the future, this experiment could be repeated using more tissue, thicker slices of for example 20-50μ and 3D features. The handcrafted features did contain some 3D features and information, but did not have enough predictive ability to perform analyses with at this point. If the amount of data were to be increased, these features might be able to tell something about differences if there are any. Using the models and looking at what features explain the most variance, or in the case of a decision tree which variables are used to make decisions, it might be possible to get a basic grip on what exact structural differences there are between bicuspid patients and tricuspid patients, if there are any.

Chapter 4

Conclusion

During this thesis, two biological problems have been described as *meso* and *micro* problems. Both of these required different approaches. A range of third party tools have been used in combination with a range of Matlab and bash scripts for processing of images. For the meso problem, a stack of 100 sequential Ulex stained microscopic scanned slides have been pre-processed, cropped several times, aligned several times and segmented. This stack of images has been converted into a 3D model and combined with a vessel reconstruction created using Movat's pentachrome. The resulting animation gave some interesting insights about the 3D structure of the capillaries, such as the fact that the vasa vasorum are directly connected to the lumen of the bigger coronary vessel. The created overlat shows the relative position of the capillary network. Using this overlay, it is possible to understand the location of the network compared to other parts of the coronary artery. Although informative, the smoothness and accuracy of the model can still be improved by prevention of damage to the specimen during the cutting and staining procedures, as well as applying methods to remove loose parts of the model. 3D Smoothing might be applied to the model as well to improve the smoothness of the model which would make the model look more natural. Fluorescence microscopy using a confocal microscope is a more reliable way to create correct 3D stacks which show only the filaments that we are looking for. Using such microscope reduces the amount of overview, but segmentation and registration problems can be solved biologically. In the end, no valid method was found to visualize actin simultaneously with collagen and elastin using paraffin sections. The combination of SHG for collagen, frozen sections, no mounting medium, phalloidin and the autofluorescence of elastin was successful, but frozen tissue was not available in larger quantities. The analysis of the final imaging steps using data-mining methods did not yield any solid conclusion about structural defects in the elastin or collagen. With scores of 0.30 on a 4-class problem and 0.70 on a 2-class problem, the models that were built did not have any significant predictive ability. This could be mainly due to the fact that only 19 patients have been used in this investigation, something that might be elaborated on in the future. The handcrafted features resulted in similar scores as using the LBP features. Advantages of using these descriptors is that they might be able to indicate where exactly structural difference originate from.

Verification using different prediction tasks like whether patients suffered from Marfan's disease and whether an image was captured from the adventitial regions or the medial

regions resulted in average LOO test prediction scores of 0.95, which showed that LBP features in conjunction with a SVM seems to be a valid method for image classification tasks like comparing different tissue samples.

To come to a correct reconstruction, we need more than image processing alone. A correct biological understanding of the target of interest allows us to select the appropriate preparation, imaging and image processing techniques which in the end lead to a biologically correct reconstruction. It is very important how the dataset is built that serves as input for the computational part. Again, the combination between biology and computer science is the key to solving this reconstruction problem.

Chapter 5

Future work

In this section, suggestions for future work are listed.

As this project was an exploratory search into the domain of 3D reconstruction, there were several limitations during this thesis. For example, existing tools were linked to save time making them, but these tools often lacked efficiency and flexibility. Also, reconstructions and investigations in this project function as a basis for future research rather than as a result alone.

Reconstructions like the capillary network included in this thesis might be used for capillary flow dynamic simulations, and the structure might be investigated more. The behavior of neovascularization can be better understood using these kinds of models. Network densities and characteristics as number of branches of capillaries, capillary thickness and others can also be calculated. This model existed of 100 section images and was 400 μm high. This could be extended to 1-2mm (250-500 sections) to result in a model with cubical dimensions, which would give a better overview of the vessel and it's capillary network. To do so, previously discussed challenges in the cutting process of consecutive slices should be solved first. Moreover, there is a significant processing capacity challenge that has to be solved. More efficient software needs to be created and in case of extremely large projects, distributed computing can be used. These models can be elaborated on by adding different structures into the model by using different stains. This project used a combination of Ulex endothelium stain and Movat's Pentachrome to visualize the vessel and the capillary network in relation to the atherosclerotic lesion and the muscle wall. Using different stains, other tissue types might be indicated as well provided that they can be combined with the other stains used in the reconstruction process, or removed completely. This process can be simplified as well using re-usable mounting medium which is easily removable. Lastly, there might be a possibility that a reconstruction like this can be created using a very thick stack, but there will be significant challenges to overcome regarding the confocal microscopy such as loss of signal, for example.

The BAV disease investigation can be elaborated upon since the research group size is relatively small for the training of an SVM model. Increasing the research groups might improve the predictive ability of the model. Data-mining methods need enough data to deal with variance. Other data-mining methods might prove to be helpful as well. For example, clustering might teach us more about the data composition. Also, deep learning methods are quite powerful and might work well for this particular problem. The imaging

methods might be improved upon as well. Using frozen tissue, it is possible to visualize all three filaments of interest. If this is combined with thicker slices and more advanced, 3D features, structural defects might be proven or ruled out definitively.

During any sort of future work, the combination of Computer Science techniques and Biological (imaging) methods will remain very important.

Acknowledgments

First of all, I would like to thank both of my supervisors, prof. Dr. Ir. F.J. Verbeek and Dr. J.H.N. Lindeman for their support and guidance throughout this thesis. Without them, I would not have been able to come to the thesis as it is now. I would like to thank LIACS, as well as the LUMC which have supported me with a place to work and access to labs for biological experiments. I would also like to thank the bio-imaging group under prof. Verbeek, which were always willing to help. Gerda Lamers has introduced me to the Confocal Laser Scanning Microscope and taught me how to use it properly. These sessions have taught me a great deal about microscopy. The people at the LUMC lab were very helpful as well. Special thanks to Marlieke Geerts, Marieke Lindeman, Melissa Zuiderwijk and Connie Janssen who helped me in the lab, as well as Annelies van der Laan who introduced me to the Multiphoton confocal microscope and helped me in the search towards a good imaging setup.

Bibliography

[1] K.T. Griffioen. An automated approach for creating 3D models out of high resolution serial microscopic scans of coronary arteries. Technical report, Leiden University, Leiden, 2017.

[2] PHILIPS. IntelliSite Ultra Fast Scanner. https://www.philips.nl/healthcare/ product/HCNOCTN442/ intellisite-ultra-fast-scanner-digital-pathology-slide-scanner, 2017.

[3] Jean-Claude G Bünzli. Lighting up cells with lanthanide self-assembled helicates. *Interface focus*, 3(5):20130032, oct 2013.

[4] Michael J Sanderson, Ian Smith, Ian Parker, and Martin D Bootman. Fluorescence microscopy. *Cold Spring Harbor protocols*, 2014(10):pdb.top071795, oct 2014.

[5] GBD 2013 Mortality GBD 2013 Mortality and Causes of Death Collaborators and Causes of Death. Global, regional, and national age-sex specific all-cause and cause-specific mortality for 240 causes of death, 1990-2013: a systematic analysis for the Global Burden of Disease Study 2013. *Lancet (London, England)*, 385(9963):117–71, jan 2015.

[6] C Davis, J Fischer, K Ley, and I J Sarembock. The role of inflammation in vascular injury and repair. *Journal of thrombosis and haemostasis : JTH*, 1(8):1699–1709, 2003.

[7] Göran K Hansson and Andreas Hermansson. The immune system in atherosclerosis. *Nature Immunology*, 12(3):204–212, 2011.

[8] Nimbe Torres, Martha Guevara-Cruz, Laura A. Velázquez-Villegas, and Armando R Tovar. Nutrition and Atherosclerosis, 2015.

[9] Russell Ross. The pathogenesis of atherosclerosis: a perspective for the 1990s. *Nature*, 362(6423):801–809, 1993.

[10] Patel A. Does the Role of Angiogenesis Play a Role in Atherosclerosis and Plaque Instability? *Anatomy & Physiology*, 04(03), 2013.

[11] K S Moulton. Plaque angiogenesis and atherosclerosis. *Current atherosclerosis reports*, 3(3):225–33, 2001.

[12] Samuel C. Siu and Candice K. Silversides. Bicuspid aortic valve disease. *Journal of the American College of Cardiology*, 55(25):2789–800, jun 2010.

[13] Katie L. Losenno, Robert L. Goodman, and Michael W A Chu. Bicuspid aortic valve disease and ascending aortic aneurysms: Gaps in knowledge, 2012.

[14] Mirko Doss, Joern Balzer, Sven Martens, Jeffrey P Wood, Gerhard Wimmer-Greinecker, Hans-Gerd Fieguth, and Anton Moritz. Surgical versus endovascular treatment of acute thoracic aortic rupture: a single-center experience. *The Annals of Thoracic Surgery*, 76(5):1465–1470, 2003.

[15] Paul W M Fedak, Subodh Verma, Tirone E. David, Richard L. Leask, Richard D. Weisel, and Jagdish Butany. Clinical and pathophysiological implications of a bicuspid aortic valve, 2002.

[16] Paul W.M Fedak, Mauro P.L de Sa, Subodh Verma, Nafiseh Nili, Pedram Kazemian, Jagdish Butany, Bradley H Strauss, Richard D Weisel, and Tirone E David. Vascular matrix remodeling in patients with bicuspid aortic valve malformations: implications for aortic dilatation. *The Journal of Thoracic and Cardiovascular Surgery*, 126(3):797–805, sep 2003.

[17] Thomas M. Tadros, Michael D. Klein, and Oz M. Shapira. Ascending aortic dilatation associated with bicuspid aortic valve. Pathophysiology, molecular biology, and clinical implications. *Circulation*, 119(6):880–890, 2009.

[18] Subodh Verma and Samuel C. Siu. Aortic Dilatation in Patients with Bicuspid Aortic Valve. *New England Journal of Medicine*, 370(20):1920–1929, may 2014.

[19] Ali Aydin, Nikolaus Desai, Alexander M J Bernhardt, Hendrik Treede, Christian Detter, Sara Sheikhzadeh, Meike Rybczynski, Mathias Hillebrand, Victoria Lorenzen, Kai Mortensen, Peter N. Robinson, Jürgen Berger, Hermann Reichenspurner, Thomas Meinertz, Stephan Willems, and Yskert von Kodolitsch. Ascending aortic aneurysm and aortic valve dysfunction in bicuspid aortic valve disease. *International journal of cardiology*, 164(3):301–5, apr 2013.

[20] A. J. Barker, M. Markl, J. Burk, R. Lorenz, J. Bock, S. Bauer, J. Schulz-Menger, and F. von Knobelsdorff-Brenkenhoff. Bicuspid Aortic Valve Is Associated With Altered Wall Shear Stress in the Ascending Aorta. *Circulation: Cardiovascular Imaging*, 5(4):457–466, 2012.

[21] Hazem Abdul-Hussien, Roeland Hanemaaijer, Robert Kleemann, Ben F J Verhaaren, J Hajo van Bockel, and Jan H N Lindeman. The pathophysiology of abdominal aortic aneurysm growth: Corresponding and discordant inflammatory and proteolytic processes in abdominal aortic and popliteal artery aneurysms. *Journal of Vascular Surgery*, 51(6):1479–1487, jun 2010.

[22] Jan H N Lindeman, Brian a Ashcroft, Jan-Willem M Beenakker, Maarten van Es, Nico B R Koekkoek, Frans a Prins, Jarl F Tielemans, Hazem Abdul-Hussien, Ruud a Bank, and Tjerk H Oosterkamp. Distinct defects in collagen microarchitecture underlie vessel-wall failure in advanced abdominal aneurysms and aneurysms in Marfan syndrome. *Proceedings of the National Academy of Sciences of the United States of America*, 107(2):862–5, jan 2010.

[23] W. S. Rasband. ImageJ. *National Institutes of Health, Bethesda, Maryland, USA.*, page http://imagej.nih.gov/ij/, 1997.

[24] Fons J. Verbeek, D. P. Huijsmans, R J Baeten, N J Schoutsen, and W. H. Lamers. Design and implementation of a database and program for 3D reconstruction from serial sections: a data-driven approach. *Microscopy research and technique*, 30(6):496–512, apr 1995.

[25] John Cupitt and Kirk Martinez. VIPS: An image processing system for large images. *Proc. SPIE*, 2663:19–28, 1996.

[26] Mahadev Satyanarayanan, Adam Goode, Benjamin Gilbert, Jan Harkes, and Drazen Jukic. OpenSlide: A vendor-neutral software foundation for digital pathology. *Journal of Pathology Informatics*, 4(1):27, 2013.

[27] Blender Foundation. Blender, 1995.

[28] Christoph Sommer, Christoph Straehle, Ullrich Kothe, and Fred A. Hamprecht. Ilastik: Interactive learning and segmentation toolkit. In *Proceedings - International Symposium on Biomedical Imaging*, pages 230–233, 2011.

[29] Fabian Pedregosa, Gaël Varoquaux, Alexandre Gramfort, Vincent Michel, Bertrand Thirion, Olivier Grisel, Mathieu Blondel, Peter Prettenhofer, Ron Weiss, Vincent Dubourg, Jake Vanderplas, Alexandre Passos, David Cournapeau, Matthieu Brucher, Matthieu Perrot, and Édouard Duchesnay. Scikit-learn: Machine Learning in Python. *Journal of Machine Learning Research*, 12(Oct):2825–2830, 2012.

[30] L. F. Borges, S. R. Taboga, and P. S. Gutierrez. Simultaneous observation of collagen and elastin in normal and pathological tissues: Analysis of Sirius-red-stained sections by fluorescence microscopy. *Cell and Tissue Research*, 320(3):551–552, 2005.

[31] Brad Chazotte. Labeling cytoskeletal F-actin with rhodamine phalloidin or fluorescein phalloidin for imaging. *Cold Spring Harbor protocols*, 2010(5):pdb.prot4947, may 2010.

[32] J. Victor Small, Klemens Rottner, Penelope Hahne, and Kurt I. Anderson. Visualising the actin cytoskeleton. *Microscopy Research and Technique*, 47(1):3–17, oct 1999.

[33] H Z MOVAT. Demonstration of all connective tissue elements in a single section; pentachrome stains. *A.M.A. archives of pathology*, 60(3):289–95, sep 1955.

[34] Movat Pentachrome Stain Kit (Modified Russell-Movat). http://www.nordicbiosite.com/sites/default/files/fields/product_insert/file/b00bc_ksc-mps-1.pdf.

[35] H Holthöfer, I Virtanen, A L Kariniemi, M Hormia, E Linder, and A Miettinen. Ulex europaeus I lectin as a marker for vascular endothelium in human tissues. *Laboratory investigation; a journal of technical methods and pathology*, 47(1):60–6, 1982.

[36] RW Dapson, C Fagan, JA Kiernan, and TW Wickersham. Certification procedures for sirius red F3B (CI 35780, Direct red 80). *Biotechnic & Histochemistry*, 86(3):133–139, 2011.

[37] K.T. Griffioen. Cappilary vessel reconstruction. https://www.youtube.com/watch?v=7FgbGxFng_I, 2017.

[38] Xiyi Chen, Oleg Nadiarynkh, Sergey Plotnikov, and Paul J Campagnola. Second harmonic generation microscopy for quantitative analysis of collagen fibrillar structure. *Nat Protoc*, 7(4):654–669, mar 2012.

[39] J.W. Beenakker. *Unravelling the collagen network of the arterial wall.* Phd thesis, Leiden University, 2012.

[40] T Ojala, M Pietikainen, and T Maenpaa. Multiresolution gray-scale and rotation invariant texture classification with local binary patterns. *IEEE Transactions on Pattern Analysis and Machine Intelligence*, 24(7):971–987, jul 2002.

[41] Navneet Dalal and William Triggs. Histograms of Oriented Gradients for Human Detection. *2005 IEEE Computer Society Conference on Computer Vision and Pattern Recognition CVPR05*, 1(3):886–893, 2004.

Appendix

A   Code

Listing 1: **generateHandcrafted.m** Script which will generate features based on all lsm files in a folder.

```
1    %%%%%%%%%%%%%%%%%%%
2    %% This script will generate features based on all lsm files in the indicated folder and write
         them to features.csv.
3    %%%%%%%%%%%%%%%%%%%
4
5    %% Cd into right dir
6    cd('C:\Dir\To\Images\');
7    addpath('C:\path\To\scripts');
8
9    dir_contents = dir('*.lsm');
10
11   %%
12   % Create new file features.csv
13   FILE = fopen('features.csv', 'w');
14   if ~FILE
15       error('We could not open file');
16   end
17
18   for i = 1:size(dir_contents,1)
19
20       disp(['loading file ' num2str(i) ' out of ' num2str(size(dir_contents,1))]);
21
22       % Write headers
23       for j = 1:size(dir_contents,2);
24           writeToCSV(FILE, dir_contents(i).name, false);
25       end
26
27       %% Come up with some interesting features and be sure to write them
28       %Read image
29       img = readim(dir_contents(i).name);
30
31       if size(size(img),2) == 4
32           % Optional: Resize image by factor 2
33           img = img(1:2:end, 1:2:end,1:2:end,:);
34
35           % Get channels
36           elastin = squeeze(img(:,:,:,1));
37           collagen = squeeze(img(:,:,:,0));
38       else
39           % Optional: Resize image by factor 2
40           img = img(1:2:end, 1:2:end,:);
41
42           % Get channels
43           elastin = squeeze(img(:,:,1));
44           collagen = squeeze(img(:,:,0));
45       end
46
47       writeToCSV(FILE, [num2str(size(elastin,1) * 2) 'x' num2str(size(elastin,2) *2)], false);
48
49       %%
50       % smooth each channel such that we get a little more even signal.
51       % Kernel size will be 2, which is fine for this resolution (1K)
52       elastin = smooth(elastin);
53       collagen = smooth(collagen);
54
55       % Get useful thresholds of collagen and actin (bit overdone such that we
56       % can use this to remove unwanted signal in the elastin channel
57       collagen_t = threshold(opening(collagen, 5));
58
59       % Remove unwanted elastin signal
```

67

```matlab
60         elastin = elastin * ~collagen_t;
61         collagen_t = ~elastin * collagen_t;
62
63      % get a threshold of the elastin such that we have a binary image
64      % containing only elastin
65      elastin_t = threshold(elastin);
66
67      % Get labels
68      elastin_labels = label(elastin_t);
69
70
71 %%      1. Length of fibers (if doable with 4 mu)
72      % measure Length (above median):
73      elastin_minmax_pos = measure(elastin_labels, [],{'minimum', 'maximum'});
74      elastin_minmax_pos = (elastin_minmax_pos.maximum - elastin_minmax_pos.minimum) .^2;
75      elastin_length = sqrt(elastin_minmax_pos(1,:) + elastin_minmax_pos(2,:));
76      % remove all below median:
77      % Fix for the high noise that was generated.
78      elastin_length_above_median = elastin_length(elastin_length > median(elastin_length));
79      elastin_mean_length_above_median = mean(elastin_length);
80
81 %    write
82      writeToCSV(FILE, elastin_mean_length_above_median, false);
83
84 %%      3. Thickness of fibers
85      % Size / length
86      % Get the size
87      elastin_size = measure(elastin_labels, [], 'size');
88
89      elastin_thickness = elastin_size.size / elastin_length;
90      elastin_mean_thickness = mean(elastin_thickness);
91      % Write
92      writeToCSV(FILE, elastin_mean_thickness, false);
93
94 %%      5. Number of elastin fibers in an image
95      num_elastin = max(elastin_labels);
96
97      % Write
98      writeToCSV(FILE, num_elastin, false);
99
100 %%      7. Percentage collagen in image
101      % Find percentage of collagen as well
102      image_total = prod(size(elastin_t));
103      collagen_pixels = sum(collagen_t);
104      collagen_perc = collagen_pixels / image_total;
105
106      % Write
107      writeToCSV(FILE, collagen_perc, false);
108
109 %%      8. Percentage elastin in image
110      % Find percentage of elastin that is present in the image
111      elastin_pixels = sum(elastin_t);
112
113      % Answer to this question is n/total.
114      elastin_perc = elastin_pixels / image_total;
115
116      % Write
117      writeToCSV(FILE, elastin_perc, false);
118
119 %% Branching pixels from bskel
120      % Use a 2D version of the image (this does not work in 3D)
121      image_2d = getBrightestImageFromStack(elastin);
122      % Take simple threshold
123      image_2d_t = threshold(image_2d);
124      % Get bskel like this:
125      img_skel = bskeleton(image_2d_t);
126      % Get branch pixels:
127      branch_pixels = getbranchpixel(img_skel);
128      num_branch_pixels = sum(branch_pixels);
129
130      writeToCSV(FILE, num_branch_pixels, false);
131
132 %%      9. Ratio collagen/elastin
133      collagen_elastin_ratio = collagen_pixels / elastin_pixels;
134
135      % Write
136      writeToCSV(FILE, collagen_elastin_ratio, true);
137
138      %% Print newline
139      fprintf(FILE, '\n');
140 end
141
142 fclose(FILE);
```

Listing 2: **cropImg.m** Script which will allow the user to sequentially crop TIFF files in the indicated directory. Loads the 5th layer of the TIFF as a thumbnail to select the correct area from after which the indicated layer is cropped using the coordinates specificied.

```matlab
function cropimg(layer, outputdir, cropObj = 0, overwrite = false)
    %% Crop images from folder (can be reused)
    %    inputs:
    %        -    layer (number)
    %        -    outputdir (string)
    %        -    OPTIONAL: cropobj (string): path to previous cropObj. If used before, this
    %             script will save such an object in the outputdir
    %        -    OPTIONAL: overwrite (bool): use if you want to redo this folder
    croppingFromFile = (cropObj ~= 0);
    if croppingFromFile
        load(cropObj);
        cropObj
    else
        cropObj = {};
        cropObj.filenames = {};
        cropObj.rects = {};
    end

    function out = contains(fnames_struct, find_string)
        for i = 1:length(fnames_struct)
            if strcmp(fnames_struct(i).name, find_string)
                out = i;
                return;
            end
        end
        out = false;
    end

    created_temp_tiff = false;
    f = dir;
    for i = 1:length(f)
        img = f(i).name
        if length(img) > 5 && img(end-4:end) == ".tiff"
            if ~croppingFromFile || contains(cropObj.filenames, img) == false
                %% Make a smaller version of the original tiff file.
                system(["vips tiffload \"" img "\" temp.tiff --page 5"]);
                created_temp_tiff = true;
                %% Read the version
                im = imread("temp.tiff");
                %% Use it to crop an ROI
                [~, rect] = imcrop(im);
                %% Close the window afterwards
                cropObj.filenames(end+1).name = img;
                cropObj.rects(end+1).rect = rect;
                close all;
            else
                rect = cropObj.rects(contains(cropObj.filenames, img)).rect;
            end

            if overwrite || ~exist([outputdir "/" img], "file")
                %% Produce a larger version of the Tiff
                %system(["vips tiffload \"" img "\" templarge.v --page " num2str(layer)]);
                %% Multiply the ROI with a power of 2 according to the level
                rect = rect * 2^(5-layer);
                %% Make int
                rect = round(rect);
                %% Execute crop!
                system(["vips crop \"" img "[page=" num2str(layer) "]\" \"" outputdir "/" img
                    "\" " num2str(rect(1)) " " num2str(rect(2)) " " num2str(rect(3)) " " num2str
                    (rect(4))]);
            end

            if created_temp_tiff
                %Remove files
                delete("temp.tiff");
                created_temp_tiff = false;
                save([outputdir "/cropObj.mat"], "cropObj");
            end
        end
    end
end
```

B Checklist

This checklist provides a set of guidelines which should be taken into consideration when conducting research into a 3D-structure related problem.

B.1 Imaging Techniques

- First off, the correct imaging technique(s) should be chosen for the problem that is investigated. This can be done taking the microscopy techniques comparison of table 3.1. It is important to be aware of the disadvantages of every method, as the imaging part is the most important part of 3D reconstruction work-flows.

- If the tissue of interest comprises a 'meso'-structure like the muscle regions in a coronary blood vessel, the most applicable method would be to use a Movat-stain or even a more specific muscle-stain and image using a whole slide scanner. This can be done using fluorescence in conjunction with a wide-field fluorescence scanner as well, though procedures are generally more complex in comparison with classical color-stains.

- When the research subject comprises smaller structures which need more specific signal to improve segmentation of local structures like individual fibers, for example, using confocal fluorescence microscopy might be an interesting approach.

B.2 Sample preparation

- Prior to sample preparation, the imaging technique should be known.

- Paraffin embedded tissue is generally easier to work with and is easier to store in comparison with frozen tissue.

- The sample preparation technique of choice depends on a few factors.

    - Availability of paraffin or frozen tissue
    - Microscopy method. If the microscopy method of choice is fluorescence microscopy and frozen tissue is available, this is the preferred choice. Otherwise, paraffin might be better because it is easier to work with.
    - Microscopy goals. Even if the microscopy method is fluorescence microscopy, the stains that are used might be compatible with paraffin embedded tissue. If so, paraffin is the preferred preparation type.

- When the goal is to create a 3D reconstruction with consecutive slices, the cutting phase is the most important step in the process. Both tissue damage prevention and correct numbering is of the utmost importance. Tissue damage can be prevented by keeping the block at 20 degrees Celcius. When working at room temperature, working with enough speed to prevent having to take the block out of the microtome is important. If the series is longer than 50 slices, it might be better working in a room with lower temperatures such that the paraffin block does not warm up.

B.3 Fluorescence microscopy

There are a few important things to think about regarding fluorescence microscopy in general, of which a few can be deducted from table 3.2.

- One of the main things that have to be taken into consideration is the preparation of the tissue. This can greatly influence the way fluorescent substances interact with tissue. For example, when tissue was embedded in paraffin for the preparation of tissue which was stained with phalloidin, the phalloidin signal was almost gone, while using frozen tissue, the signal was very clear.

- The choice of mounting medium can be important as well. Xylene can have a negative effect on the signal of certain stains or imaging methods as SHG.

- Knowledge about the imaging target. In this project, imaging targets were elastin, actin and collagen. Sirius red was used as a collagen stain, and every other methods' results were compared to this first result. In the end, Sirius red appears to stain collagen and actin simultaneously, meaning that this comparison was incorrect.

B.4 3D reconstruction

There are a few software packages which are very helpful when creating a 3D reconstruction.

- If a fluorescence microscope is used, the Zen software suite of Zeiss is a valuable tool, optionally in combination with ImageJ which has a bit more options.

- Creating a 3D reconstruction with consecutive slide scans requires more knowledge.

  - The Vips toolbox in conjunction with Matlab can be used for image manipulation operations like scaling or cropping
  - ImageJ plugins can be used for registration
  - ImageJ can also be used for segmentation, but Ilastik is a very helpful tool as well.
  - TDR is very helpful software for the final 3D model creation and creates accurate, smooth and interpolated 3D reconstructions. If the image stack is segmented using imageJ, a 3D model can be generated using ImageJ's 3D viewer as well, but the final quality will be less in comparison with TDR.